2019

Investigating the role of N-methyl-D-aspartate receptor subunit exchange in visual recognition memory

Ying Li
yli11@wellesley.edu

Investigating the role of N-methyl-D-aspartate receptor subunit exchange in visual recognition memory

Ying Li

Submitted in Partial Fulfillment
of the
Prerequisite for Honors
in Biochemistry
under the advisement of Dr. Peter S.B. Finnie
and Dr. Elizabeth S.C. Oakes

May 2019

Acknowledgements

I would like to express my sincere gratitude to my off-campus advisor, Dr. Peter Finnie, who has kindly given me endless support and encouragement throughout my college career. Thank you for your incredible guidance, inspiration, patience, and wisdom. You helped me grow as a critical thinker and challenged me during my process of research and writing.

Thank you to my on-campus advisor and major advisor, Dr. Elizabeth Oakes, for your enthusiasm, and mentorship. I genuinely appreciate your endless supply of invaluable academic and personal advice.

I would also like to thank Dr. Mark F. Bear for providing me with the amazing opportunity to work in the Bear Lab. The experiences I have gained in your lab have not only inspired me, but also strengthened my passion for science and research. Thank you to my colleagues and friends in the Bear Lab—Dr. Arnold Heynen, Dr. Ming-fai Fong, Dr. Héctor De Jesús-Cortés, Taekeun Kim, Dustin Hayden, Maia Lee, Rebekah Waldman, Jocelyn Yao, and Lisandro Martin—for your support and contributions to this project, from friendly conversations to experimental design to data collection and analysis.

A warm thank you to my thesis committee members, Dr. Melissa A. Beers and Dr. Barbara S. Beltz, for your thoughtful suggestions on this project and for encouraging me to think inquisitively. I would also like to thank Dr. Angela C. Carpenter, who enthusiastically accepted my invitation to be my thesis visitor.

To my biochemistry family—Linnea Fischer, Camilla Koczara, Susan Liu, Zijing Li, Andrea Sama, Victoria Condon, Michelle Li, Rachel Utomo, Subha Baniya, Justine Hsu, and Mayla Thompson—thank you for all the memories in Sage and the numerous conversations we have had throughout the years.

To Lyon Qiao: thank you for the many laughs and late-night calls. I cannot thank you enough for your motivation and belief in me.

Thank you to all my friends, especially Julia Wainwright and Helena Yan, for your encouragement. This thesis would not have been made possible without you all.

Lastly, thank you to my family for the constant love and support. I could not have gotten this far without you.

Table of Contents

Acknowledgements 1
List of Figures 4
1 Abstract 5
2 Introduction 6
2.1 Memory 6
2.2 Long-term Potentiation in the Murine Visual Cortex 7
2.3 Stimulus-specific Response Potentiation (SRP) 7
2.4 Orientation-selective habituation (OSH) 10
2.5 Role of NMDA Receptors in Memory 12
2.6 Investigating the involvement of NDMA receptor subunit exchange in SRP 20
3 Methods & Materials 21
3.1 Animal Husbandry 21
3.2 Headpost and Electrode Implantation 21
3.3 Viral Injection 22
3.4 Pharmacologic Injection 23
3.5 Recording Rig Design 24
3.6 Stimulus Presentation 25
3.7 Behavioral Data Acquisition and Analysis 27
3.8 Electrophysiological Data Acquisition and Analysis 27
3.9 Visual Cortex Extraction 27
3.10 Perfusion 28
3.11 Immunohistochemistry 28
3.12 Western Blot and Image Analysis 29
3.13 Statistical Analysis 30
4 Results 32
4.1 NR2B to NR2A subunit exchange during the acquisition of SRP 32
4.2 Effect of NR2B knockout on the acquisition of SRP and OSH 35
4.3 Effect of NR2B pharmacological inhibition on the acquisition of SRP and OSH 42
4.4.1 Effect of NR2B inhibition via CP-101,606 on SRP and OSH 42
4.4.2 Effect of NR2B inhibition via Ro 25-6981 on SRP and OSH 48

5 Discussion 53
5.1 NMDA receptor subunit composition in V1 neurons does not change during SRP 53
5.2 Genetic ablation of NR2B was unable to reveal the role of NR2B in SRP and OSH ... 55
5.3 High concentration DMSO occludes the acquisition, but not the consolidation, of visual memory 58
5.4 Ro 25-6981 inhibition of NR2B shows that NR2B may not necessary for SRP and OSH 62
6 Future directions 65
7 Conclusions 66
8 References 68
9 Appendices 71
Appendix A: Abbreviations 71
Appendix B: Supplementary Figures 72

List of Figures

Introduction
Figure 1: Repeated exposure to familiar phase-reversing, sinusoidal grating visual stimulus visual stimulus increases the magnitude of visually evoked potentials (VEP) measured in layer 4 of V1 8
Figure 2: Repeated exposure to familiar phase-reversing, sinusoidal grating visual stimulus decreases the magnitude of visually evoked fidget behaviors (vidgets) 11
Figure 3: Schematic representation of NMDA receptor activation by co-agonists glycine and glutamate 13
Figure 4: The structure of NMDA receptors 15
Figure 5: Experience-dependent subunit exchange alters the composition and electrochemical properties of NMDA receptors 18

Methods & Materials
Figure 6: Location of headpost and electrode implantation on the skull of mice 22
Figure 7: Recording rig to standardize visual stimulus presentation to head-fixed mice 24

Results
Figure 8: NR2A/NR2B ratios in the visual and frontal cortices do not change significantly following the acquisition of SRP 34
Figure 9: Virally induced GFP expression in CaMKII-expressing cells was diffuse in the visual cortex of control mice 35
Figure 10: Virally induced Cre-GFP expression in CaMKII-expressing cells was sparse and restricted to the primary visual cortex of injected mice 36
Figure 11: Spatial acuity and contrast sensitivity are mostly preserved in NR2B KO mice relative to control animals 37
Figure 12: Loss of NR2B may reduce baseline VEP magnitude 41
Figure 13: High concentration DMSO vehicle, not CP-101,606, likely occludes the acquisition, but not consolidation, of visual memory 44
Figure 14: Selective NR2B antagonist Ro 25-6981 does not appear to attenuate SRP or OSH 48

Discussion
Figure 15: Ifenprodil, which is structurally similar to Ro 25-6981 and traxoprodil (i.e., CP-101,606), binds to the GluN1/GluN2B (i.e. NR1/NR2B) interface 59

Appendices
Figure S1: NR2B and NR2A are upregulated in equal proportion in the frontal cortex with increasing visual experience despite no apparent change in total NMDA receptor number 72
Figure S2: NR2B and NR2A are upregulated in equal proportion in the visual cortex with increasing visual experience despite no apparent change in total NMDA receptor number 73

1 Abstract

Visual memory is a complex neurophysiological process wherein visual inputs are transduced and encoded within networks of synapsing neurons. At the core of this system are neurotransmitters and postsynaptic receptors, including N-methyl-D-aspartate (NMDA) receptors, which are necessary for visual memory in mice. Interestingly, with age there is a predictable, visual experience-dependent replacement of NMDA receptor subunit NR2B by a second subunit, NR2A. Both subunits have been implicated in regulating potentiation in the murine primary visual cortex (V1) in response to visual stimulus in other forms of plasticity, such as ocular dominance. The goal of this project was to characterize NMDA receptor subunit composition changes during the acquisition of visual memory and to elucidate the role of NR2B in stimulus-specific response potentiation (SRP) and orientation-selective habituation (OSH), which are electrophysiological and behavioral manifestations of visual memory, respectively. To this end, we measured NR2A and NR2B protein levels via Western blot in mice before and after six days of exposure to a sinusoidal grating stimulus. We also evaluated SRP and OSH in mice in which NR2B was selectively deleted by Cre recombinase or pharmacologically inhibited by either CP-101,606 or Ro 25-6981. Our preliminary findings indicate that NMDA subunit exchange in V1 is minimal during the acquisition of visual memory. We observed that the loss of NR2B does not appear to impact SRP or OSH, suggesting that the subunit does not play a role in visual memory, although these biological effects are obscured by high variance and small sample sizes. Finally, we report that DMSO—used as a pharmacological vehicle—may inhibit the acquisition, but not the consolidation of visual memory. Our work here on characterising NMDA receptor subunit NR2B explores one aspect of the biochemical basis of plasticity in V1 and suggests alternative mechanisms that underlie visual memory that warrant further investigation in order to fully understand learning and memory.

2 Introduction

2.1 Memory

"Memory in youth is active and easily impressible; in old age it is comparatively callous to new impressions, but still retains vividly those of earlier years." (Charlotte Brontë)

Writing from the 1840s, Charlotte Brontë reflected on memory and its intimate relationship with age. Today, memory is recognized as a beautifully intricate process, involving the cross-talk of complex neural networks and biomolecular signaling events, that underlies human cognition. Environmental cues—sight, sound, touch, smell, and taste—are integrated and recorded into memory for retrieval at a later time. For simplicity, this volume will specifically focus on visual memory, its biochemical basis, and its physiological manifestations.

It would be remiss to begin this discussion without recognizing that animals learn from their sensory environment. During the 1940s, for instance, Donald O. Hebb remarked that rodents kept as pets seemingly outperformed their counterparts raised in cages on problem solving tests, suggesting that stimuli in the environment could shape behaviors independently of artificial learning, including Pavlovian conditioning (Hebb, 1947). Then, in the 1960s David Hubel and Torsten Wiesel observed that monocular deprivation, or the intentional disruption of sight through one eye in binocular animals, led to cellular and anatomical changes within the brain (Wiesel and Hubel, 1963). Specifically, following monocular deprivation, groups of neurons found within the primary visual cortex (V1) that typically receive visual input from one or both eyes, termed ocular dominance columns, only received input from a single eye; ocular dominance columns that received input from the open eye were enlarged in V1 and expanded into space within the cortex normally occupied by ocular dominance columns corresponding to the contralateral eye (Wiesel and Hubel, 1963). Taken together, these observations suggest that environmental stimuli can shape the brain and impact cortical function.

2.2 Long-term Potentiation in the Murine Visual Cortex

In neuroscience, it is widely accepted that patterned stimulation of the brain can strengthen the synapses activated by the stimulus, in a process termed long-term potentiation (LTP) (Bliss and Lomo, 1973). The inverse process, long-term depression (LTD), or the progressive weakening of synapses can also occur, typically following lower-frequency stimulation. These two opposing processes are thought to form the basis of learning and memory, and contribute to synaptic plasticity, or the ability of neurons to alter the strengths of their chemical synapses. LTP has been observed in many sensory modalities across several species, including humans (Fahle and Morgan, 1996; Furmanski et al., 2004; Gilbert et al., 2001; Karni and Bertini, 1997; Poggio et al., 1992). Notably, plasticity changes in the form of electrophysiological signals in V1 have been observed in mice exposed to familiar visual stimuli that resemble canonical presentations of LTP (Cooke and Bear, 2010; Frenkel et al., 2006). V1 is a bilaterally paired region of the cortex in the occipital lobes that receives visual input from the eyes via the optic nerves and dorsal lateral geniculate nucleus (dLGN) of the thalamus. Interestingly, it has been demonstrated in later work that LTP in V1 occurs independently of structures traditionally associated with memory, including the hippocampus. Indeed, pharmacological hippocampal ablation does not affect the ability of V1 to undergo an LTP-like process in response to visual stimuli (unpublished work). This observation suggests that neural networks within V1 are capable of undergoing plasticity changes in response to visual stimuli, which might underlie familiarization, habituation, and object recognition.

2.3 Stimulus-specific Response Potentiation (SRP)

Electrical activity in the brain has been correlated with specific stimuli and cognitive processes. Visual recognition is no exception. In mice, recognition of familiar visual stimuli has been reported to manifest electrophysiologically as the progressive increase in cortical activity in V1, a

phenomenon dubbed stimulus-specific response potentiation (SRP) first observed incidentally in mice (Frenkel et al., 2006; Sawtell et al., 2003). In this paradigm, repeated exposure to the same phase-reversing, sinusoidal grating visual stimulus (a series of lines presented at a fixed angle) elicits a predictable increase in the overall amplitude of visually evoked potentials (VEPs), which measure the strength of cortical responses (**Fig. 1**). VEPs are obtained by measuring electrical activity in mice in response to visual stimuli via implanted electrodes, and VEP magnitudes are calculated by averaging the trough-peak amplitudes of VEP waveforms. For instance, over a five-day period, the mean amplitude of VEPs have been reported to double (261.1 µV on day one compared to 144.8 µV on day five) (Cooke and Bear, 2010).

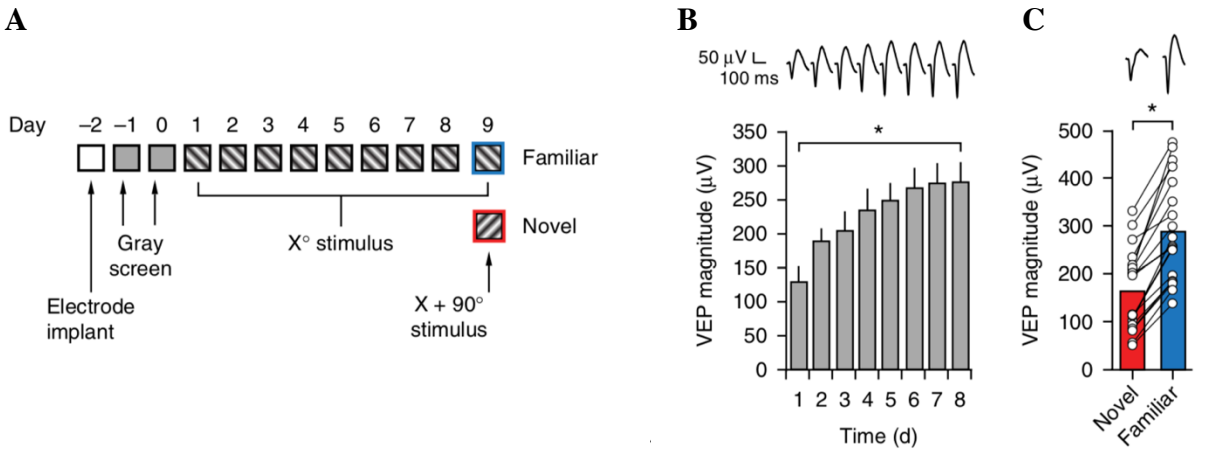

Figure 1: Repeated exposure to familiar phase-reversing, sinusoidal grating visual stimulus visual stimulus increases the magnitude of visually evoked potentials (VEP) measured in layer 4 of V1. (**A**) Head-fixed mice were exposed to the same stimulus for eight days. On day 9, mice were either shown a familiar stimulus (outlined in blue) or a novel stimulus (outlined in red). (**B**) VEP magnitudes, which were recorded on each day while mice were exposed to the familiar stimulus, increased with repeated exposure. Bars represent averaged amplitudes from VEP waveforms obtained from mice (n = 19). Average VEP waveforms are also provided above the graph. Vertical scale bar represents 50 µV; horizontal scale bar represents 100 ms. (**C**) VEP magnitudes decrease when mice are exposed to novel stimulus orientation on day 9 relative to VEP magnitudes measured on day 8 (red), while VEP magnitudes continue to increase when mice are exposed to familiar stimuli on day 9 (blue). Bars represent averaged amplitudes from VEP waveforms obtained from mice (n = 19). Circles represent VEP magnitudes measured in individual mice shown familiar (blue) and novel (red) stimuli, while lines represent the change in VEP magnitude between conditions. Figure adapted from Cooke et al. (2015).

Strikingly, exposure to a novel stimulus orientation elicits VEPs of smaller amplitude, relative to the familiar orientation. Indeed, even subtle differences in the presented visual stimulus have been shown to reduce the amplitude of VEPs, suggesting that at a neurophysiological level, mice are able to recognize and distinguish between similarly oriented visual stimuli. To illustrate this specificity, lines that deviate from familiar by as little as 5˚ elicit significantly smaller VEP amplitudes. Taken together, these observations support the notion that synaptic potentiation in response to repeated exposure to familiar stimuli is highly specific and can be observed via SRP (Cooke and Bear, 2010; Frenkel et al., 2006).

In addition to its selectivity to stimuli, SRP has been shown to be specific to the eye viewing the stimulus. Monocular exposure to a stimulus elicited SRP in the trained, but not the untrained eye (Frenkel et al., 2006), suggesting that changes in plasticity are largely driven by a small number of neurons that respond exclusively to visual signals from the trained eye. It is worth noting that SRP is not confined to the early postnatal critical period, after which plasticity is diminished and neural circuitry underlying visual memory is cemented (Frenkel et al., 2006). Indeed, progressive enhancements in VEP amplitudes can still be observed in adult mice beyond the traditional ocular dominance "critical period" (Frenkel et al., 2006).

Given that SRP co-occurs with local plasticity changes in response to visual stimuli, it has been suggested that SRP is a manifestation of LTP. Two lines of evidence support this position: (1) the induction of thalamocortical LTP (including V1) by theta burst electrical stimulation (TBS), which involves repetitive magnetic pulses that elicit changes in electrical activity, in the dLGN both mimics and occludes SRP (and vice versa). Stated otherwise, changes to VEP magnitudes following TBS resemble those seen in mice that have undergone SRP. Moreover, mice treated with TBS are unable to undergo SRP when shown the same stimulus as during TBS, suggesting

that LTP and SRP share similar biological processes. (2) Disrupting the maintenance of LTP via zeta-inhibitory peptide (ZIP) interference of calcium-dependent kinase PKMζ, which is necessary for LTP, reduces VEP amplitudes in V1 after prior induction of SRP (Cooke and Bear, 2010). These findings suggest that LTP in V1 and its associated neurophysiological changes in response to familiar visual stimulus lead to the appearance of SRP. Therefore, SRP could provide a convenient *in vivo* assay of LTP in mice exposed to visual stimulation.

2.4 Orientation-selective habituation (OSH)

In addition to SRP, which provides an electrophysiological readout for visual recognition, a second phenomenon called orientation-selective habituation (OSH) has been reported to emerge in parallel (Cooke et al., 2015). When exposed to visual stimuli, mice exhibit a distinct fidgeting behavior, dubbed the "vidget," that decreases in magnitude with familiarity to a given stimulus (**Fig. 2**). Indeed, when mice are exposed to the same phase-reversing, sinusoidal grating visual stimulus, the average magnitude of vidgets, accessed via piezoelectric sensor placed under the forepaws, fell by over 64% across eight days. When trained mice were exposed to a novel visual stimulus on the ninth day, the magnitude of vidgets increased by almost 100% relative to the magnitude of vidgets observed during the previous day, suggesting that the behavioural response is specific to a given visual stimulus (Cooke et al., 2015). These observations mirror those observed in SRP, where the amplitude of VEPs increases with familiarity to a given visual stimulus (Cooke and Bear, 2010; Cooke et al., 2015).

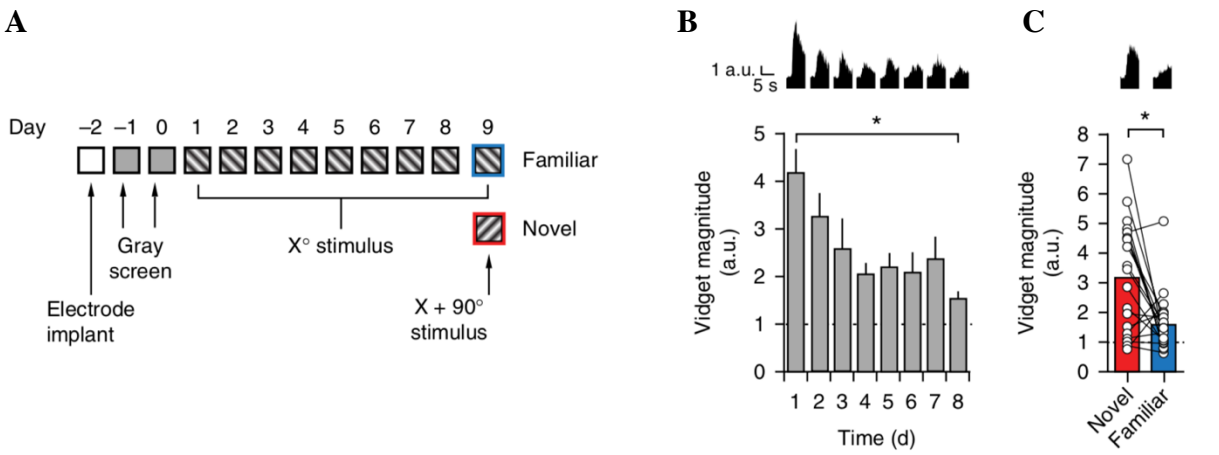

Figure 2: Repeated exposure to familiar phase-reversing, sinusoidal grating visual stimulus decreases the magnitude of visually evoked fidget behaviors (vidgets). (**A**) Head-fixed mice were exposed to the same stimulus for eight days. On day 9, mice were shown both a familiar stimulus (outlined in blue) and a novel stimulus (outlined in red). (**B**) Vidget magnitudes, which were recorded each day while mice were exposed to the familiar stimulus, decrease with repeated exposure. Bars represent averaged amplitudes from piezoelectrical signals obtained from vidgets in mice (n = 19). Average vidget waveforms are also provided above the graph. Vertical scale bar represents 1 a.u.; horizontal scale bar represents 5 s. (**C**) Vidget magnitudes increase when mice are exposed to novel stimuli on day 9 (red) relative to vidget magnitudes measured on day 8, while vidget magnitudes remain relatively stable when exposed to familiar stimuli on day 9 (blue). Bars represent averaged amplitudes from vidget waveforms obtained from mice (n = 19). Circles represent vidget magnitudes measured in individual mice shown familiar (blue) and novel (red) stimuli, while lines represent the change in vidget magnitude between conditions. Figure adapted from Cooke et al. (2015).

Like SRP, OSH is eye-specific, supporting the notion that neural circuits modified by visual input are not shared downstream of segregated monocular projections from dLGN (Cooke et al., 2015). In the case of OSH, when each eye is habituated with a differently oriented stimulus and subsequently exposed to the contralateral stimulus, vidget magnitudes increase in each eye, suggesting that the neural circuitry that receives input from each eye recognizes this new stimulus as novel. In the case of SRP, following exposure to the contralateral stimulus, VEP magnitudes decrease in each eye, corroborating observations above (Cooke et al., 2015).

As SRP and OSH occur simultaneously during habituation, OSH is thought to be a behavioral manifestation of the LTP-like process in V1. The elimination of LTP by ZIP peptide, which was

previously shown to preclude SRP, similarly abolishes OSH in mice, supporting the hypothesis that this visually-evoked form of LTP manifests electrophysiologically as SRP and behaviorally as OSH (Cooke et al., 2015). Consistent with this finding, unlike many other non-stimulus-specific reflexive behaviors, OSH depends on neuronal activity within V1. Treatment of V1 with $GABA_A$ receptor agonist muscimol, which reduces neuronal activity by hyperpolarizing the neuron, thereby inhibiting the formation and propagation of action potentials, reduced both the magnitude of VEP amplitudes and the magnitude of vidgets in mice exposed to familiar stimuli (Cooke et al., 2015). The same result was observed in mice in which V1 signalling was perturbed by the local activation of channelrhodopsin-2 in parvalbumin-expressing GABAergic interneurons, which activate these inhibitory neurons, thereby suppressing neural activity, supporting the notion that SRP and OSH are driven by neuronal circuits located within V1 (Cooke et al., 2015). Taken together, these results demonstrate that SRP and OSH might arise from the occurrence of LTP in V1 in response to habituation to visual stimuli.

2.5 Role of NMDA Receptors in Memory

At the basis of the neuronal networks that permit memory formation are neurotransmitters, which primarily transmit neuronal impulses from presynaptic neurons to postsynaptic neurons. The amino acid glutamate is a neurotransmitter that binds to glutamatergic receptors including N-methyl-D-aspartate (NMDA) receptors on the postsynaptic membrane (McBain and Mayer, 1994). A large volume of literature has implicated the activity of NMDA receptors in initiating synaptic plasticity and the reorganization of neuronal circuits involved in learning and memory in the CNS. As with other ionotropic receptors, NMDA receptors are ligand-gated ion channels activated by glutamate and glycine, permitting the passive movement of non-specific cations through the channel (**Fig. 3**). Though the movement of cations, including sodium, calcium, and potassium,

through the channel requires ligand binding, net flux is ultimately dependent on membrane potential, which contributes to the chemiosmotic gradient and regulates the binding of magnesium ions to specific sites within the channel. These magnesium ions effectively block the flow of other cations unless they are displaced by membrane depolarization (McBain and Mayer, 1994). Generally, the activation of NMDA receptors results in the net flow of positively charged sodium and calcium ions into cells.

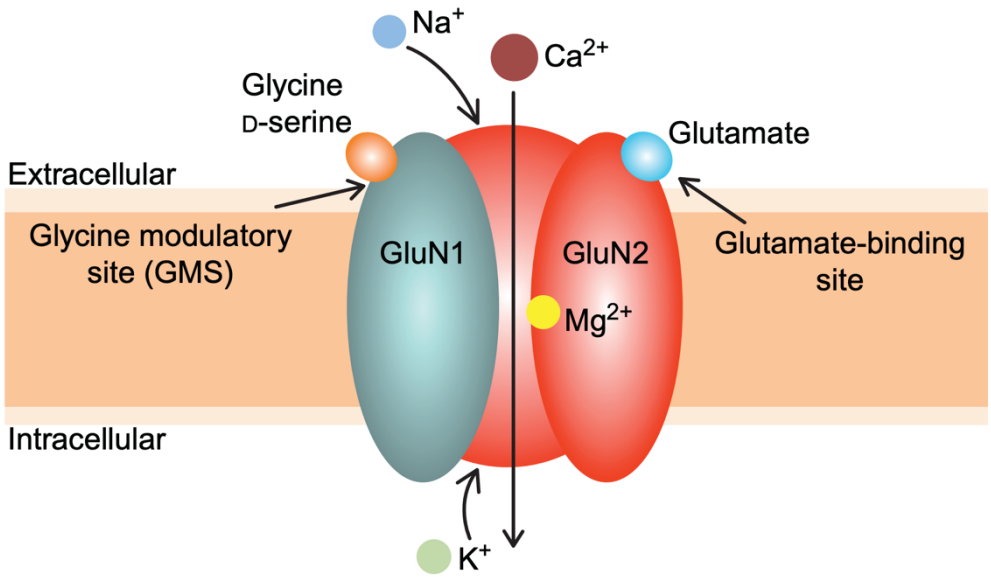

Figure 3: Schematic representation of NMDA receptor activation by co-agonists glycine and glutamate. NMDA receptor is an ionotropic ligand-gated cation channel that is activated by the binding of glycine (orange) to subunit NR1 (labeled GluN1 above) and glutamate (turquoise) to subunit NR2 (labeled GluN2). Magnesium ions (yellow) also bind to subunit NR2 and prevent the movement of sodium (blue), calcium (maroon), and potassium (green) ions across the neuronal membrane. Displacement of magnesium ions by membrane depolarization (not shown) permits the net flow of positive ions into the cell along their chemiosmotic gradient. Figure adapted from Balu (2016).

Structurally, NMDA receptors are heteromeric transmembrane proteins composed of four peptide subunits (**Fig. 4A**), including two obligatory NR1 subunits and two variable NR2 or NR3 subunits. Among each type of subunit, different subtypes also exist (e.g., NR2A-D encoded by four different genes, NR1-1a/b-NR1-4a/b formed by alternative splicing of the GRIN1 mRNA),

contributing to the overall diversity of NMDA receptors in the brain (McBain and Mayer, 1994). On the whole, the different subunits share similar structural elements: an extracellular N-terminus and four transmembrane domains. NMDA receptor subunits tend to vary in amino acid sequence within the intracellular C-terminus, which has been shown to be important in interacting with intracellular proteins, including protein kinases and phosphatases (**Fig. 4B**) (McBain and Mayer, 1994). NR1 subunits (approximately 920 amino acid residues, 103.4 kDa) are known to bind glycine, while NR2 subunits have been shown to bind glutamate and contribute to interactions with magnesium ions (**Fig. 3**). Consistent with these observations, it has been posited that NR2 subunits are largely responsible for regulating the electrochemical properties of NMDA receptors (McBain and Mayer, 1994). In the context of V1 plasticity changes, two NR2 subtypes—NR2A (1442 amino acid residues, 162.8 kDa) and NR2B (1456 amino acid residues, 163.2 kDa)—are most commonly discussed since they are the most abundant subunits in the mammalian forebrain (McBain and Mayer, 1994).

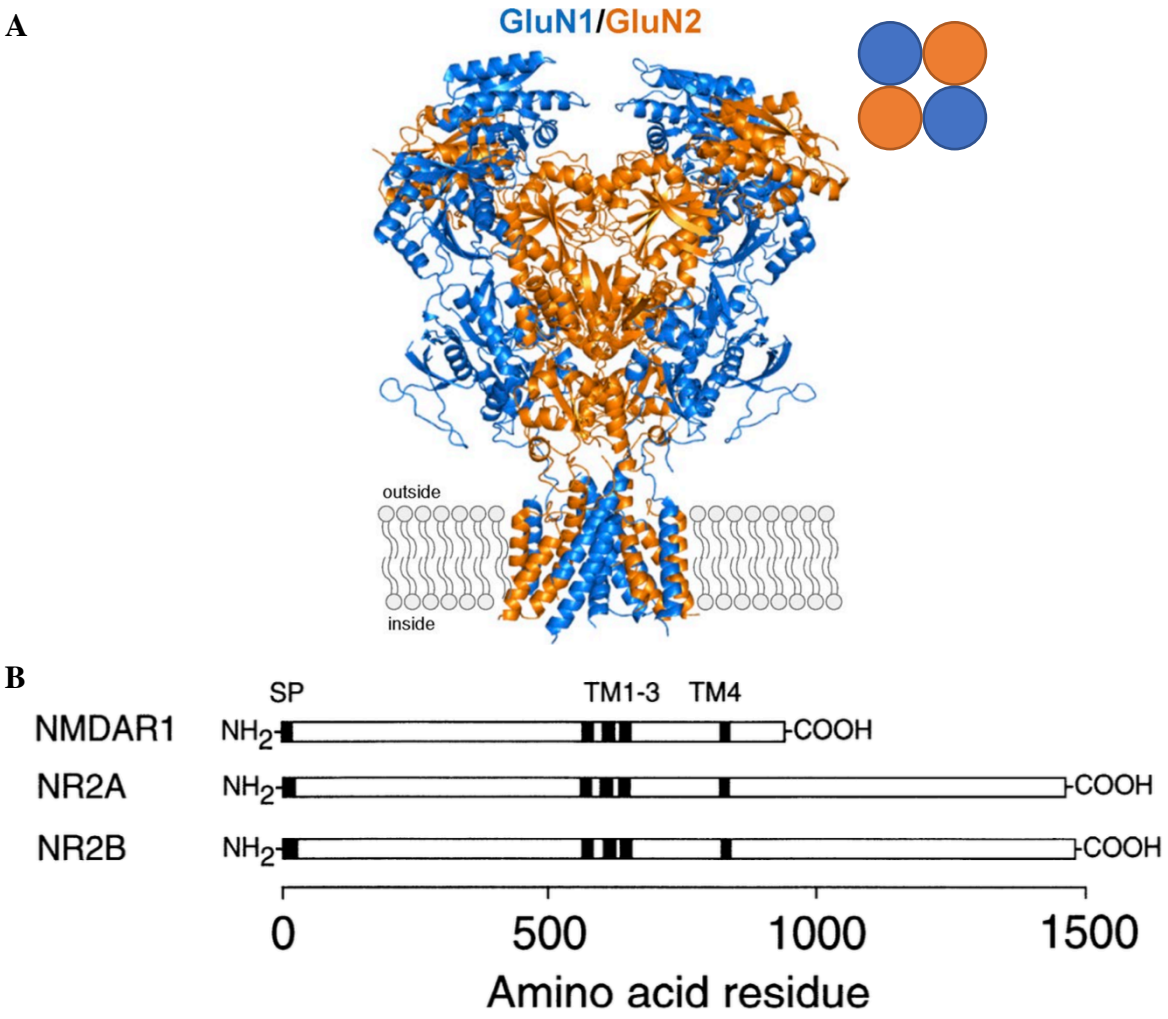

Figure 4: The structure of NMDA receptors. (**A**) A ribbon structure of the heterotetrameric NMDA receptor containing two subunits of NR1 (blue) and two subunits of NR2 (orange). (**b**) Comparison between amino acid sequences of NR1 (labeled NMDAR1), NR2A, and NR2B. Note the number and location of transmembrane domains (black boxes labeled as TM1-3, TM4) and the length of the peptides. SP: signal peptide. Figures adapted from (**a**) Hansen et al. (2018) and (**B**) McBain & Mayer (1994).

As in other regions of the brain, NMDA receptors have been demonstrated to be necessary for SRP in V1. For instance, pharmacological inhibition of NMDA receptor by antagonist 3-(2-carboxypiperazin-4-yl)propyl-1-phosphonic acid (CPP) has been demonstrated to abolish SRP and therefore, LTP, in mice (Frenkel et al., 2006). Moreover, the targeted deletion of obligatory NMDA receptor subunit NR1 in V1 similarly eliminated SRP (Frenkel et al., 2006), suggesting

that the activity of NMDA receptors is necessary for the manifestation of electrophysiological changes associated with LTP. These findings are consistent with prior observations of the role of NMDA receptors in ocular dominance plasticity in mice (Sawtell et al., 2003). Classically, binocular regions of V1 receive signals largely from the contralateral eye with a minor contribution from the ipsilateral eye. Monocular deprivation of the contralateral eye strengthens visual input from the ipsilateral eye via a process dependent on the activation of NMDA receptors (Sawtell et al., 2003). Indeed, changes to ocular dominance plasticity are abolished in mice containing targeted NR1 subunit deletions, suggesting a possible role of NMDA receptors in reorganizing neuronal circuits following changes to visual stimulus input (Sawtell et al., 2003).

Consistent with the findings described previously, the activity of NMDA receptors in V1 is also required for OSH, the behavioral manifestation of LTP in V1 (Cooke et al., 2015). Targeted deletion of NMDA receptor subunit NR1 in V1 abolishes OSH and prevents mutant mice from distinguishing between familiar and novel stimuli (Cooke et al., 2015). Similarly, the inhibition of NMDA receptors in V1 via localized delivery of antagonist 2-amino-5-phosphonopentanoate (AP5) prevented the acquisition of OSH and SRP in mice prior to exposure to visual stimuli (Cooke et al., 2015). Taken together, these observations support the notion that NMDA receptors are required for the establishment and maintenance of OSH, SRP, and therefore, LTP in V1.

In addition to the demonstrated role of NMDA receptor activity in V1 that underlies LTP and complex processes related to visual memory formation and maintenance, NMDA receptors undergo a predictable biochemical change during the life time of vertebrates. Indeed, during prenatal and early post-natal developmental periods (first five weeks in mice), NMDA receptors in the forebrain contain primarily NR2B subunits, while NMDA receptors in the brain during late post-natal developmental periods corresponding to the end of juvenile plasticity contain relatively

more NR2A subunits (**Fig. 5A**), suggesting that the gradual replacement of NR2B subunits by NR2A subunits is a normal physiologic process related to the development and aging of mammals, including mice (Cho et al., 2009; Quinlan et al., 1999). It must be noted that cells do not actively exchange NR2A subunits for NR2B subunits in existing NMDA receptors on the postsynaptic membrane. Prior work has shown that NMDA receptors localized in newly established cortical and thalamic synapses contain a mixture of NR2B and NR2A, suggesting that NR2A may be preferentially expressed following the formation of new connections in response to novel learning (Liu et al., 2004). This finding is supported by the observation that the developmental NMDA receptor subunit exchange is abolished in dark-reared animals (i.e., lacking visual input) (Quinlan et al., 1999). Moreover, exposure to light (and the surrounding visual environment) causes a rapid increase in NR2A subunit composition in V1, suggesting that the transition from NR2B to NR2A is experience-dependent and likely underlies alterations to the electrochemical properties of NMDA receptors that occur with LTP and visual memory acquisition (Quinlan et al., 1999).

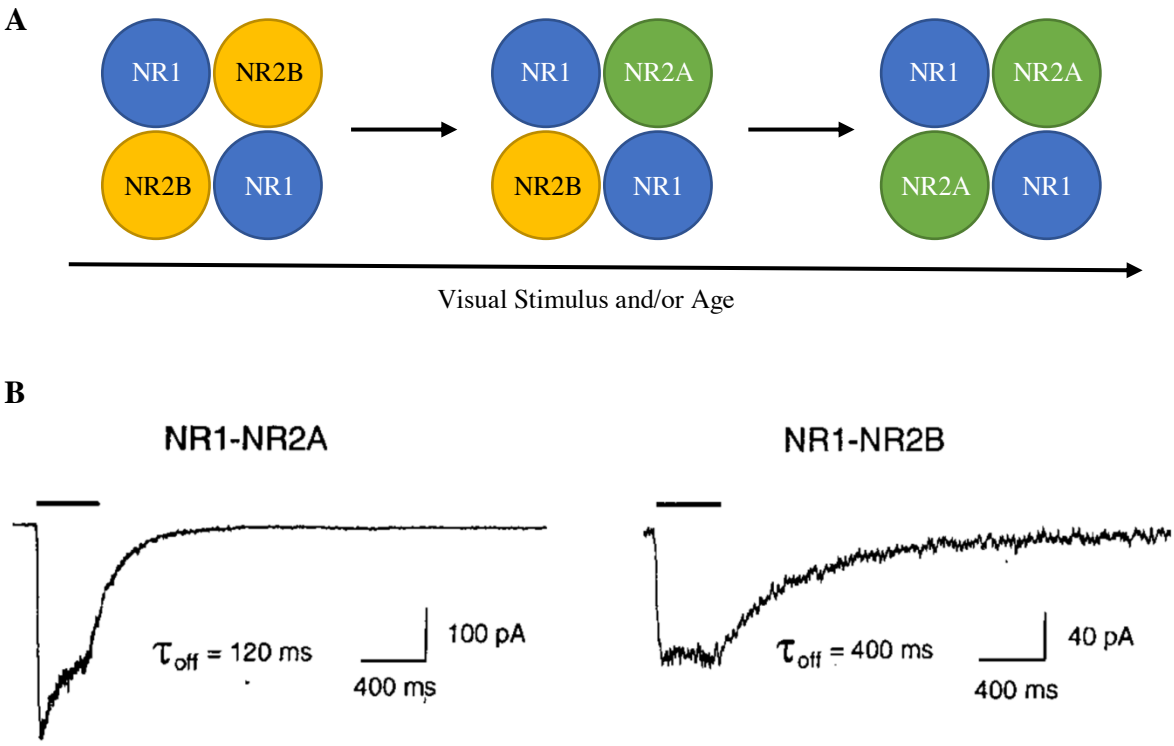

Figure 5: Experience-dependent subunit exchange alters the composition and electrochemical properties of NMDA receptors. (**A**) A schematic representation of the NR2B-to-NR2A transition with increasing visual stimulation and age. (**B**) The presence of NR2A causes NMDA receptors to generate more rapid excitatory post-synaptic currents (smaller offset decay time constant, τ) compared to NR2B-containing NMDA receptors. Figure (**B**) adapted from Monyer et al. (1994).

Before exploring the functional relationship between NMDA receptor subunit composition and processes that govern LTP in V1, it is worth contrasting the physical properties of NR2B-containing NMDA receptors and NR2A-containing NMDA receptors. While NR2B-containing NMDA receptors and NR2A-containing NMDA receptors do not differ significantly in terms of calcium ion permeability, the offset decay time constant of NR2A-containing NMDA receptors is almost three-to-four times smaller than that of NR2B-containing NMDA receptors (Monyer et al., 1994), suggesting that NR2A-containing NMDA receptors mediate shorter excitatory post-synaptic currents than NR2B-containing NMDA receptors (**Fig. 5B**). Stated otherwise, NR2B-containing receptors remain open for a longer period of time. Consistent with these findings,

increasing the NR2B/NR2A subunit ratio in NMDA receptors also increases the duration of NMDA receptor excitatory post-synaptic currents (Quinlan et al., 1999). The converse is also true, supporting the notion that NMDA receptor subunit composition determines its electrochemical properties.

Interestingly, it has been claimed that the activation of NR2A-containing NMDA receptors is necessary for LTP, or synaptic strengthening, while the activation of NR2B-containing NMDA receptors, which remain open longer than NR2A-containing NMDA receptors, is necessary for LTD, or synaptic weakening (Massey et al., 2004). This hypothesis is consistent with the fact that LTP and LTD are both invoked by post-synaptic excitatory currents and calcium influx, with the former elicited by higher frequency stimulation and the latter elicited by lower frequencies. The threshold between LTP and LTD is defined as the modification threshold, which is thought to shift according to NMDA structure. It has been proposed that NMDAR subunit composition controls the modification threshold for bidirectional synaptic plasticity, although the evidence of this role depends on the nature of experimental manipulations used in each study. For instance, lowering the NR2A/NR2B ratio has been shown to reduce the threshold necessary to induce LTP in murine V1 (Cho et al., 2009; Philpot et al., 2007). Furthermore, the genetic disruption of NR2A in cortical layer 4 of V1 has also been shown to reduce the LTD/LTP threshold, thereby promoting LTP in murine V1, in a dosage-dependent manner (Cho et al., 2009). Taken together, these data suggest that the experience-dependent shift in NMDA receptor NR2 subunit identity underlies changes in V1 cortical plasticity by altering the electrophysiological threshold that determines the stimulation properties eliciting LTP versus LTD.

2.6 Investigating the involvement of NDMA receptor subunit exchange in SRP

Given the exquisite role of NMDA receptor subunit exchange in regulating the electrochemical properties of NMDA receptor, which have been shown to underlie SRP and OSH, there is great interest in understanding how the biochemical changes in NMDA receptor composition occur during familiarization with visual stimuli and the acquisition and consolidation of visual memory. The goal of this present work is foremost to characterize the NR2B-to-NR2A NMDA receptor shift in V1 during SRP induced by repeated exposure to the same visual stimulus via Western blot. Since visual deprivation is associated with reduced NR2A/NR2B ratio, we hypothesize that SRP is correlated with a rise in NR2A relative to NR2B.

Moreover, since the NR2B-to-NR2A transition is experience-dependent and correlated with a loss of V1 cortical plasticity, this project also aims to determine whether the NR2B-to-NR2A transition, specifically, stabilizes SRP during the familiarization of visual stimuli by the targeted disruption of NR2B via genetic and/or pharmacological means. Our goal is to understand how SRP and OSH change as a result of the deletion of floxed NR2B alleles specifically in V1 excitatory cells via Cre-mediated recombination and the selective inhibition of NR2B-containing NMDA receptors via NR2B selective antagonists CP-101,606 and Ro 25-6981 (Menniti et al., 1998) in mice repeatedly exposed to the same set of visual stimuli.

3 Methods & Materials

3.1 Animal Husbandry

All procedures involving live mice and mouse tissues were approved by the Committee on Animal Care (CAC) at MIT. For NMDA receptor subunit composition and pharmacological inhibition experiments, wild-type male and female C57BL/6N mice aged postnatal days 27-29 (p27-29) were obtained from Charles River Laboratory or bred from existing mouse lines housed at the Picower Institute for Learning and Memory Mouse Colony. For NR2B conditional knockout experiments, C57BL/6N mice aged p56-66 engineered with homozygous NR2B conditional alleles (*Grin2b*$^{fl/fl}$) (Sanz-Clemente et al., 2013) were obtained from breeders generously donated by Professor Roger A. Nicoll at UCSF.

3.2 Headpost and Electrode Implantation

In each experiment, mice were implanted with a headpost to fix head position and standardize the viewing angle for visual stimuli. Mice were first anesthetized with 3% isoflurane (chamber) or 1.5% isoflurane (nosecone). The scalp of each mouse was then shaved, cleaned with betadine and 70% ethanol, and injected subdermally with 1% lidocaine hydrochloride. Mice were also injected with 1 mg/kg meloxicam and 0.1 mg/kg buprenorphine subcutaneously to provide analgesia. A small incision was made to the scalp to expose the skull. Following the incision, a steel headpost was attached to the skull anterior to the bregma along the sagittal suture using cyanoacrylate glue (Loctite® 454).

For the electrophysiology experiments, mice were also implanted bilaterally with electrodes into layer 4 of binocular V1 in order to measure V1 electrical activity. To implant the electrodes into V1, burr holes (<0.5 mm) were drilled in the skull over the visual cortex perpendicular to the sagittal suture. For the NR2B conditional knockout experiment, burr holes were drilled 3.05 mm

lateral to lambda to account for larger brain size in older animals (p56-66). For all other experiments, burr holes were drilled 2.95 mm lateral to lambda (p27-29 animals). Tungsten electrodes (FHC, 75 µm in diameter) were then inserted bilaterally 450 µm below the surface of the cortex. A reference (ground) electrode was also implanted in the right frontal cortex (anterior to the coronal suture, right of the sagittal suture) at a depth of ~250-500 µm subdurally. Electrodes were affixed using Loctite® 454 superglue, and the headpost and electrodes were covered with dental cement. Mice were monitored postoperatively for distress and were allowed to recover for 3 days. During this recovery period, the mice were injected subcutaneously with 0.1 mg/kg buprenorphine 6 hours following surgery and 1 mg/kg meloxicam every 24 hours over the 3 postoperative days.

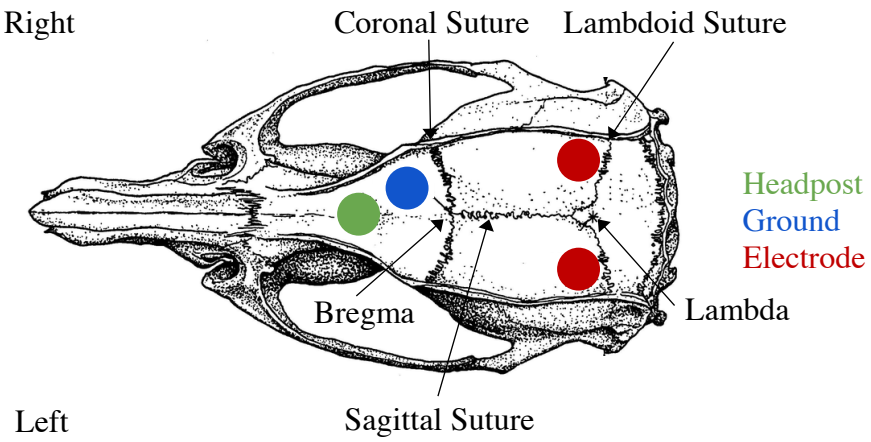

Figure 6: Location of headpost and electrode implantation on the skull of mice. The headpost (green) was affixed to the skull anterior to the bregma along the sagittal suture, while the ground electrode (blue) was implanted anterior to the coronal suture and right of the sagittal suture. Electrodes (red) were implanted 2.95-3.05 mm lateral to lambda and perpendicular to the sagittal suture. Figure adapted from Paxinos and Watson (1998).

3.3 Viral Injection

Adeno-associated viruses (AAV8) were used to locally infect CaMKII-expressing cells of the visual cortex to knockout NR2B in *Grin2b*$^{fl/fl}$ mice. These mice were injected with AAV8

expressing either Cre recombinase and green fluorescent protein (GFP) under the control of the promoter of the gene encoding alpha-Ca^{2+}/calmodulin-dependent protein kinase II (CaMKII) (NR2B KO; AAV8-CaMKII-Cre-GFP) or GFP alone under the control of the same promoter (control; AAV8-CaMKII-GFP); both viruses were obtained from the University of North Carolina viral core.

Viral injections were delivered during the same surgical session as headpost and electrode implantation for the NR2B conditional knockout experiment. Viral injections were delivered using a glass pipette and Nanoject III system (Drummond Scientific) at three cortical depths below the surface of the skull: 250 µm, 450 µm, and 750 µm. Injections were delivered perpendicular to the sagittal suture and 2.90 mm from lambda bilaterally. At each depth, 9 injections of 9.6 nL were delivered 30 seconds apart at a rate of 46 nL/s (86.4 nL total), and 2 min were allowed between repositioning for depth. Mice were monitored postoperatively for distress and were allowed to recover for 3 days. During this initial recovery period, the mice were injected subcutaneously with 0.1 mg/kg buprenorphine 6 hours following injection and 1 mg/kg meloxicam every 24 hours for the 3 postoperative days. Mice were then allowed 4 weeks of recovery before further experimentation to allow for robust viral expression.

3.4 Pharmacologic Injection

Intraperitoneal injections were performed in accordance with CAC and Bear Lab guidelines. In one set of pharmacological inhibition experiments, mice were injected intraperitoneally with CP-101,606 (10 mg/kg) (Sigma-Aldrich, SML0053) dissolved in 75% v/v DMSO in Milli-Q sterile water or vehicle alone. In a second set of pharmacological inhibition experiments, mice were injected with Ro 25-6981 (10 mg/kg) (Sigma-Aldrich, SML0495) dissolved in isotonic saline

or vehicle alone. Further experimentation commenced either 30 (Ro 25-6981) or 60 (CP-101,606) min following injections to allow for drug uptake, diffusion, and binding to NR2B.

3.5 Recording Rig Design

To standardize visual stimulus presentation across different mice and stimulation conditions, we employed a recoding rig described in Cooke et al. (2015). To immobilize mice and prevent changes in viewing perspective, mice were placed into a cylindrical tube and their heads were restrained via implanted headpost, respectively. Implanted electrodes used to measure VEPs and piezoelectric sensors placed under the forepaws of the mouse to measure vidgets were then connected to the recording system (Plexon OmniPlex Recorder-64). Phase reversing grating visual stimuli were presented to the head-restrained mouse via a digital display that was placed 20 cm away from the mouse and centered, in order to occupy 92˚ × 66˚ of the visual field.

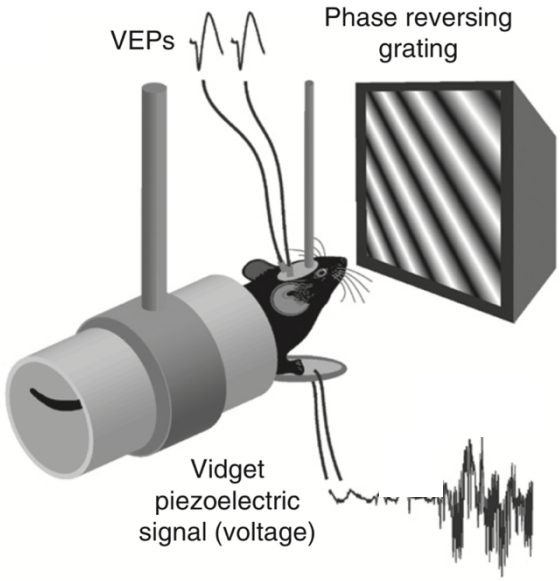

Figure 7: Recording rig to standardize visual stimulus presentation to head-fixed mice. Implanted electrodes and piezoelectric sensor placed underneath the forepaws measure to VEP and vidget magnitudes, respectively. Figure adapted from Cooke et al. (2015).

3.6 Stimulus Presentation

Phase-reversing grating visual stimuli were generated using custom code written in MATLAB and C++ by Jeff Gavornik that permitted control of the spatial frequency, angle, contrast, number of sets of phase reversals (flip/flops), number of sessions, interstimulus interval, and phase reversal frequency of visual stimuli. Prior to all experiments, mice were acclimatized to the recording rig by being head-fixed and exposed to grey screen for 30 min per day for 2 days. For NMDA receptor subunit composition experiments, mice were presented with 300 s of grey screen before one of four different visual stimulation protocols. One group of negative control mice received 5 blocks of grey screen stimulus for 6 days. The experimental group were presented with a 2 Hz, 0.05 cycles/degree, 100% contrast, 45˚ sinusoidal grating visual stimulus over 5 blocks of 100 phase reversals with 30 s between blocks and 500 ms between phase reversals for 6 days. Another negative control group received 5 days of grey screen stimulus followed by a single day of a 2 Hz, 0.05 cycles/degree, 100% contrast, 45˚ sinusoidal grating visual stimulus over 5 blocks of 100 phase reversals with 30 s between blocks and 500 ms between phase reversals. The final negative control group received a single day of a 2 Hz, 0.05 cycles/degree, 100% contrast, 45˚ sinusoidal grating visual stimulus over 5 blocks of 100 phase reversals with 30 s between blocks and 500 ms between phase reversals followed by 5 days of grey screen stimulus. The total amount of time elapsed during visual stimulation was the same in all groups.

For NR2B conditional knockout experiments, mice were presented with 300 s of grey screen before a 2 Hz, 0.05 cycles/degree, 100% contrast, 45˚ sinusoidal grating visual stimulus over 5 blocks of 100 phase reversals with 30 s between blocks and 500 ms between phase reversals for 6 consecutive days. On day 7, mice were presented with 300 s of grey screen before pseudorandomly viewing interweaved blocks of 45˚ and 135˚ sinusoidal grating visual stimulus at 2 Hz, 0.05 cycles/degree, 100% contrast, and 5 blocks of 100 phase reversals with 30 s between blocks and

500 ms between phase reversals. For spatial acuity tests performed as part of the NR2B conditional knockout experiment, mice were presented with 300 s of grey screen before a set of 2 Hz, 100% contrast, 15˚ sinusoidal grating visual stimuli over 3 blocks of 50 phase reversals with 30 s between blocks and 500 ms between phase reversals at different spatial frequencies, presented in pseudorandomly interleaved order: 0.05, 0.1, 0.2, 0.4, 0.5, 0.6, and 0.7 cycles/degree. For contrast sensitivity tests performed as part of the NR2B conditional knockout experiment, mice were presented with 300 s of grey screen before a set of 2 Hz, 0.05 cycles/degrees, 165˚ sinusoidal grating visual stimuli over 3 blocks of 50 phase reversals with 30 s between blocks and 500 ms between phase reversals at different contrasts presented in pseudorandomly interleaved order: 1, 2, 6, 12, 25, 50, and 100%.

For the NR2B pharmacological inhibition experiment, mice were presented with 300 s of grey screen before different visual stimulus conditions. On day 1, mice were presented with a 2 Hz, 0.05 cycles/degree, 100% contrast, 135˚ sinusoidal grating visual stimulus over 5 blocks of 100 phase reversals with 30s between blocks and 500 ms between phase reversals. Mice were injected immediately after this exposure, and 30-60 min later, mice were shown a 2 Hz, 0.05 cycles/degree, 100% contrast, 45˚ sinusoidal grating visual stimulus over 5 blocks of 100 phase reversals with 30s between blocks and 500 ms between phase reversals. On day 3, mice were presented with a set of 2 Hz, 0.05 cycles/degree, 100% contrast sinusoidal grating visual stimuli over 5 blocks of 100 phase reversals with 30s between blocks and 500 ms between phase reversals at 45˚, 75˚, and 135˚. On day 7, mice were presented with a set of 2 Hz, 0.05 cycles/degree, 100% contrast sinusoidal grating visual stimulus over 4 blocks of 100 phase reversals with 30s between blocks and 500 ms between phase reversals at 45˚, 75˚, 105˚, and 135˚.

3.7 Behavioral Data Acquisition and Analysis

Behavioral vidget responses were measured via piezoelectric sensor placed under the forepaws of head-restrained mice presented with visual stimuli. Head-fixed behavior was recorded continuously and automatically without experimenters in the same room as the mice. Vidget magnitudes were obtained by calculating the root mean square of the voltage signal during each 5 s interval following the onset of each block of visual stimulation. All vidget magnitudes were normalized to the forepaw movements recorded 2 s prior to the delivery of visual stimuli, reported in arbitrary units (a.u). Behavioral analysis was conducted with custom MATLAB scripts by an experimenter blind to the experimental condition.

3.8 Electrophysiological Data Acquisition and Analysis

Electrical activity in V1 elicited by visual stimulus were recorded via implanted extracellular local field electrodes connected to the electrophysiology recording system (Recorder-64) (1-kHz sampling and a 500-Hz low-pass filter). VEP data were analyzed using custom MATLAB scripts by an experimenter blind to the experimental condition. VEP magnitudes were calculated as the average peak-trough N1-to-P1 component difference measured during a 300 ms period for each distinct stimulus presented on each day. All VEP magnitudes are reported in μV.

3.9 Visual Cortex Extraction

For biochemical analysis, mice were deeply anesthetized using 3% isoflurane (chamber). Anesthetised animals were decapitated using large scissors, and whole brains were extracted by dissecting the fascia and skull. Extracted brains were incubated immediately in chilled, carbogen-infused artificial cerebrospinal fluid (ACSF, 87 mM NaCl, 3 mM KCl, 1.25 mM NaH_2PO_4, 26 mM $NaHCO_3$, 0.5 mM $CaCl_2$, 7 mM $MgCl_2$, 20 mM *D*-(+)-glucose, 1.3 mM *L*-ascorbate, and 75 mM sucrose) (Sigma-Aldrich) on a petri dish. Brains were cut along the transverse fissure using a

scalpel to separate the cerebrum from the cerebellum, pons, medulla, and brain stem. The two hemispheres of the brain were then separated by cutting along the central sulcus using a scalpel. The brain was then cut posterior to the thalamus to remove the midbrain. The brain was carefully dissected to isolate and remove the visual and frontal cortices. Dissected tissues were flash frozen with liquid nitrogen and stored at -80˚C for further analysis.

3.10 Perfusion

For immunohistochemistry, mice were anesthetized with Fatal-Plus (60 mg/kg pentobarbital) via intraperitoneal injection and perfused intracardially with 4% paraformaldehyde in 0.1 M phosphate buffered saline. Following perfusion, mice were decapitated using large scissors, and skin and fascia were dissected from the skull. The brain was then extracted from the skull and post-fixed in 4% paraformaldehyde in 0.1 M phosphate buffered saline for 24 hours at 4˚C.

3.11 Immunohistochemistry

After fixation in 4% paraformaldehyde in 0.1 M phosphate buffered saline, brains were sectioned into 50 μm-thick coronal slices using a vibratome. Slices were treated with blocking solution (0.1% Triton-X in phosphate buffered saline) and shaken for 10 min at room temperature. Following two phosphate buffered saline washes, slices were treated with Nissl (NeuroTrace 640/660; Invitrogen; 1:100 dilution) and Hoescht stain (Hoescht 33342; ThermoFisher Scientific; 1:10,000 dilution) and shaken for 20 min at room temperature. Slices were then washed once with blocking solution and three times with phosphate buffered saline. Slices were mounted with ProLong Diamond antifade media (ThermoFisher). Images were acquired via confocal fluorescence microscopy via 4x and 10x objective lenses (Olympus). The confocal filter sets were 405 nm (Hoechst), 488 nm (GFP), and 647 (far-red).

3.12 Western Blot and Image Analysis

Western blot was performed in accordance with established laboratory procedures. Thawed brain tissues were treated with 100 μL of radioimmunoprecipitation assay (RIPA) buffer prior to tissue homogenization. Homogenized tissue was centrifuged for 15 min at 16100 rcf, and the supernatant was extracted and diluted 1:20 in RIPA buffer. As protein concentration in each extraction can vary with sample handling and size, a bicinchoninic acid (BCA) protein assay was performed. 150 mg of protein in RIPA buffer were then treated with 5% v/v β-mercaptoethanol (βME) in a sodium dodecyl sulfate (SDS) solution.

10 mg of total protein treated with βME/SDS were resolved on a 7.5% polyacrylamide gel (BioRad) in Tris/glycine/SDS buffer (150 V, 3A, and 300 W for 48 min) along with Protein Dual Color Standards. Proteins within the gel were transferred to the nitrocellulose membrane via Bio-Rad Trans-Blot Turbo Transfer System machine in transfer buffer (Trans-Blot Turbo Transfer Buffer and 20% ethanol in water). Following confirmation of protein transfer with red Ponceau S solution, the nitrocellulose membrane was washed once with water and TBS-T buffer and incubated in Odyssey Blocking Buffer. Nitrocellulose membranes were then excised with a scalpel and treated with primary antibody solution (0.1% TWEEN-20 and 0.03-0.1% primary antibody in blocking buffer) at 4˚C overnight on rotators. Primary antibodies used in this protocol are listed here: monoclonal mouse anti-NR2B antibody (MA1-2014, lot# SK260648; Invitrogen; 1 mg/mL), monoclonal rabbit anti-NR1 antibody (ab109182, lot# GR3174915-7; Abcam; 0.483 mg/mL), monoclonal rabbit anti-NR2A antibody (ab124913, lot# GR25196-12; Abcam; 1.903 mg/mL), and monoclonal mouse anti-β-actin antibody (A5441, lot# 026M4780V; Sigma; 2 mg/mL).

Following three washes with TBS-T buffer, the nitrocellulose membrane was treated with secondary antibody solution (0.1% TWEEN-20, 0.02% IRDye 800CW donkey anti-rabbit

antibody (LI-COR), and 0.01% IRDye 680RD donkey anti-mouse antibody (LI-COR) in blocking buffer) and shaken for 60 min. After three washes with TBS-T and then with TBS to remove unbound or weakly bound antibodies, the membrane was imaged on the ChemiDoc MP Imaging System with 800CW (green) and 680RD (red) channels.

Bands corresponding to NR2A/NR2B/NR1 and β-actin were detected based on molecular weight in the gel (165 kDa, 166 kDa, 105 kDa, and 13.5 kDa, respectively). The intensity of each band was estimated using ChemiDoc MP software tools and automatically adjusted to account for background fluorescence. Band volumes corresponding to NR2A, NR2B, and NR1 were first normalized to the band volumes of β-actin from each sample. β-actin-normalized band volumes corresponding to NR2A and NR2B were then normalized to β-actin-normalized band volumes corresponding to NR1 from each sample. The ratio of NR2A to NR2B band volumes, each normalized to β-actin and NR1, were calculated to determine the relative subunit enrichment from each sample. Data analysis for relative protein concentration and NR2A/NR2B were performed on MATLAB.

3.13 Statistical Analysis

Data collected are presented graphically with individual data points/bars representing group means with error bars represent standard error of the mean (SEM). Statistical analysis was primarily performed on GraphPad PRISM from data generated in MATLAB. For the NMDA receptor subunit composition protein quantification, one-way repeated-measures analysis of variance (ANOVA) were performed, with samples matched by western blot membrane. For all other experiments, including genetic and pharmacological inhibition of NR2B, two-way repeated measures ANOVA were conducted with the test day or visual stimulus as the within-subjects factor, and treatment condition as a between groups factor. To further explore differences between

groups or stimuli analyzed via two-way repeated-measures ANOVA, Sidak's multiple comparison test was also used *post-hoc*. A 0.05 alpha value was used as the threshold for significance, and we reported the exact *p* values obtained from our statistical analysis except when $p < 0.0001$. Adjusted *p* values obtained from Sidak's correction for multiple comparisons for individual comparisons were also reported. Although it is statistically inappropriate to compare groups with small sample sizes (n = 2-5), as we are not properly able to conduct tests for normality and homogeneity of variance, we nevertheless reported parametric tests, such as ANOVA, to analyze our data.

4 Results

In order to better understand the biochemistry underlying NMDA receptor function in visual memory, we sought to describe NMDA receptor subunit exchange during familiarization with visual stimuli and elucidate the function of subunit NR2B in SRP and OSH, manifestations of visual memory. To achieve our first aim, we exposed mice to different sets of visual stimulation protocols for six days, isolated mouse V1 tissue, and measured NR2A and NR2B proteins levels via Western blot. With regards to our second goal, we approached the investigation of NR2B in three ways: 1) we generated NR2B loss-of-function animals by genetically ablating NR2B in binocular V1 specifically using Cre recombinase, 2) we inhibited NR2B systemically via intraperitoneal injection of selective NR2B antagonist CP-101,606, and 3) we inhibited NR2B systemically via intraperitoneal injection of a second selective NR2B antagonist, Ro 25-6981. All NR2B loss-of-function animals and matched control animals were then subjected to visual stimulation protocols for seven days, and SRP and OSH were measured in all animals via bilaterally implanted electrodes in binocular V1 and piezoelectric forepaw sensors, respectively. Here, we report the key findings from our experiments.

4.1 NR2B to NR2A subunit exchange during the acquisition of SRP

In order to track changes in NMDA receptor subunit composition during the acquisition of visual memory, we subjected male and female wild-type (p27-29) C57BL/6N mice to 1 of 4 six-day visual stimulation protocols and subsequently measured NMDA subunit protein expression in V1 via Western blot. Visual stimulus protocols included a) daily exposures to a static grey screen stimulus, which was intended to serve as a true negative control, b) daily exposure to a full-field oriented grating stimulus phase-reversing at 2 Hz (100 phase reversals), that was previously shown to induce and fully saturate SRP (Cooke et al., 2015) and two additional conditions, in which mice

were exposed to the phase-reversing grating stimulus only on c) day 6 or d) day 1 of training (**Fig. 8A**). The latter conditions were intended to dissociate the effects of stimulus repetition and time since training, as biochemical changes might occur gradually after experience. NR2A and NR2B quantities were determined from Western blot analysis and normalized against NR1 and β-actin levels. In V1, we observed no statistical difference in the NR2A/NR2B ratio among the different groups (n = 5) (one-way repeated-measures ANOVA, $F_{2,8} = 1.205$, $p = 0.3488$) (**Fig. 8B**), suggesting that NMDA receptor composition may not change significantly during the short time course of our experimental design (six days). Cortical tissue from the frontal cortex was also subjected to Western blot analysis in order to serve as a control for non-specific changes in NMDA receptor composition (**Fig. 8C**). Generally, the frontal cortex is less responsive to simple visual cues than is V1, so NMDA receptor composition should not change significantly across visual stimulus conditions (one-way repeated-measures ANOVA, $F_{2,8} = 0.4338$, $p = 0.6624$). However, we observed considerable variability in frontal cortical NMDA receptor composition, likely reflecting the small sample size (**Fig. 8C**). Interestingly, while there were no statistically significant differences in the NR2A/NR2B ratio between mice treated with the SRP protocol and mice treated with the three control conditions in both regions of the cortex, there is a general trend toward increased NR2A and NR2B expression in both V1 and the frontal cortex of mice treated with the SRP protocol (**Fig. S1**; **Fig. S2**), though these differences are admittedly not statistically significant. Taken together, our preliminary findings suggest that the subunit composition of NMDA receptors in V1 of C57BL/6N mice does not change significantly during the acquisition of SRP over six days beginning on p27-29.

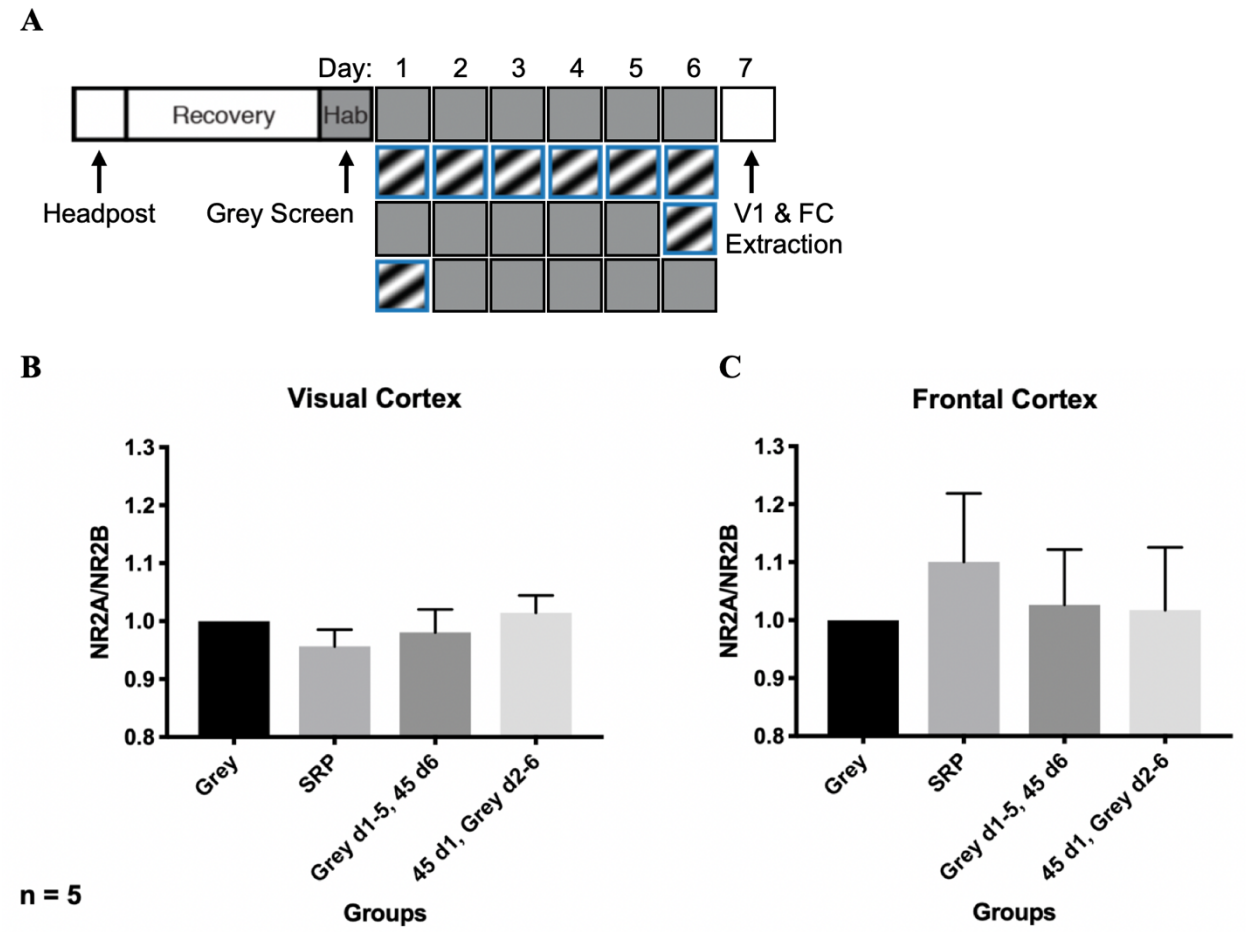

Figure 8: NR2A/NR2B ratios in the visual and frontal cortices do not change significantly following the acquisition of SRP. (**A**) Mice were surgically affixed with a headpost for head stabilization. Following recovery, mice were presented with a grey screen over 2 days to acclimatize mice to the recording rig before exposure to one of four experimental conditions: a) static grey screen stimulus daily for 6 days (n = 5); b) 100 phase reversals of a full-field, 45° grating stimulus distributed into 5 blocks daily for 6 days (SRP; n = 5); c) static grey stimulus daily for 5 days followed by 5 blocks of 45° grating stimulus on day 6 (n = 5); d) 45° grating stimulus (five blocks) on day 1 followed by a static grey stimulus daily for the remaining 5 days (n = 5). (**B**) The NR2A/NR2B ratio determined via Western blot of visual cortical tissue does not differ significantly among the four experimental groups (n = 5). Plotted data has been normalized to the NR2A/NR2B ratio of the grey screen negative control group for each Western blot membrane (for each brain region, tissue from an equal number of animals from each group were loaded into every gel). (**C**) The NR2A/NR2B ratio in frontal cortical tissue does not differ significantly among the four groups of mice included in the experiment (n = 5). All statistical analysis was performed via one-way repeated-measures ANOVA, with samples matched by blot. Error bars in all graphs represent SEM.

4.2 Effect of NR2B knockout on the acquisition of SRP and OSH

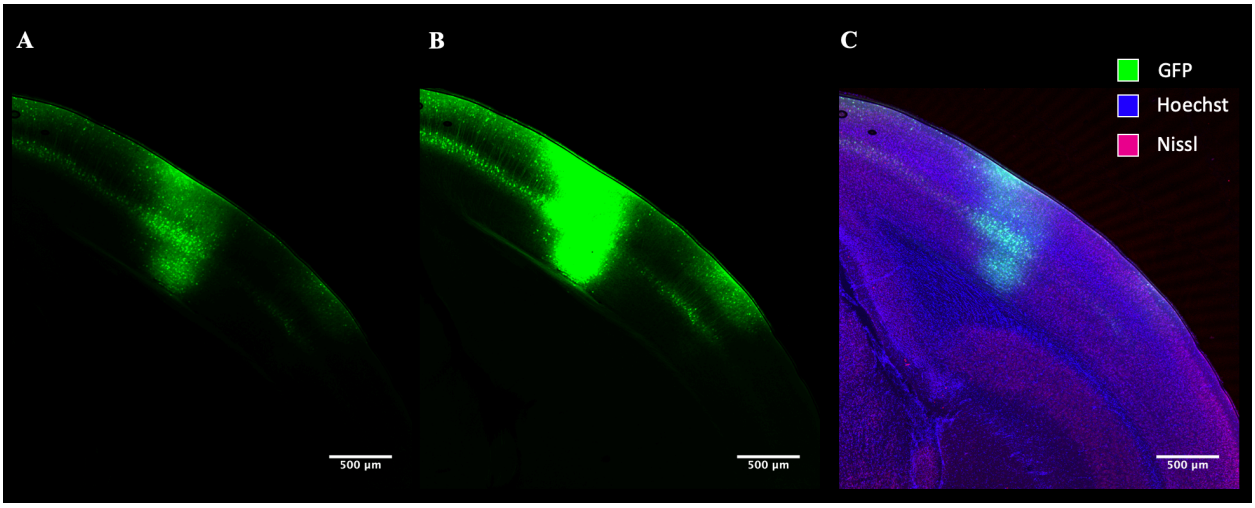

Figure 9: Virally induced GFP expression in CaMKII-expressing cells was diffuse in the visual cortex of control mice. (**A**) GFP expression (green) in mice injected with AAV8-CaMKII-GFP in the binocular region of V1 was robust and detectable in multiple regions of the cortex, including V1, by confocal microscopy. (**B**) Re-imaged region of interest from panel A with higher sensor sensitivity to detect weaker GFP signals throughout cortex. (**C**) Overlay of panel A with GFP, Hoechst (blue, DNA, 1:10,000 dilution), and Nissl (red, neuronal cell bodies, 1:100 dilution).

Our overarching hypothesis is that the NR2A/NR2B ratio regulates the ability of the NMDA receptor to initiate cortical synaptic plasticity in response to experience. Thus, we predicted that the NR2A/NR2B ratio would modulate the acquisition of SRP and, therefore, the formation of visual memory. To test whether NR2B-containing NMDA receptors are necessary for SRP and OSH, we sought to determine the effects of a genetic loss of NR2B subunits. To do so, C57BL/6 mice modified to contain LoxP sites flanking the endogenous NR2B gene (*Grin2b*) were locally injected with a virus (AAV8-CaMKII-Cre-GFP) at multiple depths within V1, to express Cre recombinase in excitatory cells within all six cortical layers. The expression of Cre recombinase in CaMKII+ cells causes the *Grin2b* gene to be excised, thereby effectively knocking out *Grin2b* in adult tissues. In order test the specificity of this approach qualitatively, we also injected the binocular region of V1 in LoxP-*Grin2b*-LoxP littermates with a control AAV8 expressing GFP under the control of a CaMKII promoter. Following experimentation, we

visualized brain tissue via confocal microscopy. Robust GFP expression was observed in the injection site, including V1, and extending to surrounding tissues, including V2, which lies adjacent to the binocular region in lateral V1 (**Fig. 9**). Within V1, strong GFP expression was observed in cells in cortical layers 2/3 and 5, but this was much more restricted in layers 4 and 6 (**Fig. 9**). Images captured at higher sensitivity demonstrated that the expression of GFP is widely observed in the cortex (**Fig. 9B**), potentially raising the concern that mice injected with an AAV8 expressing Cre recombinase will lose NR2B expression in tissues other than V1, reducing the selectivity of our manipulation.

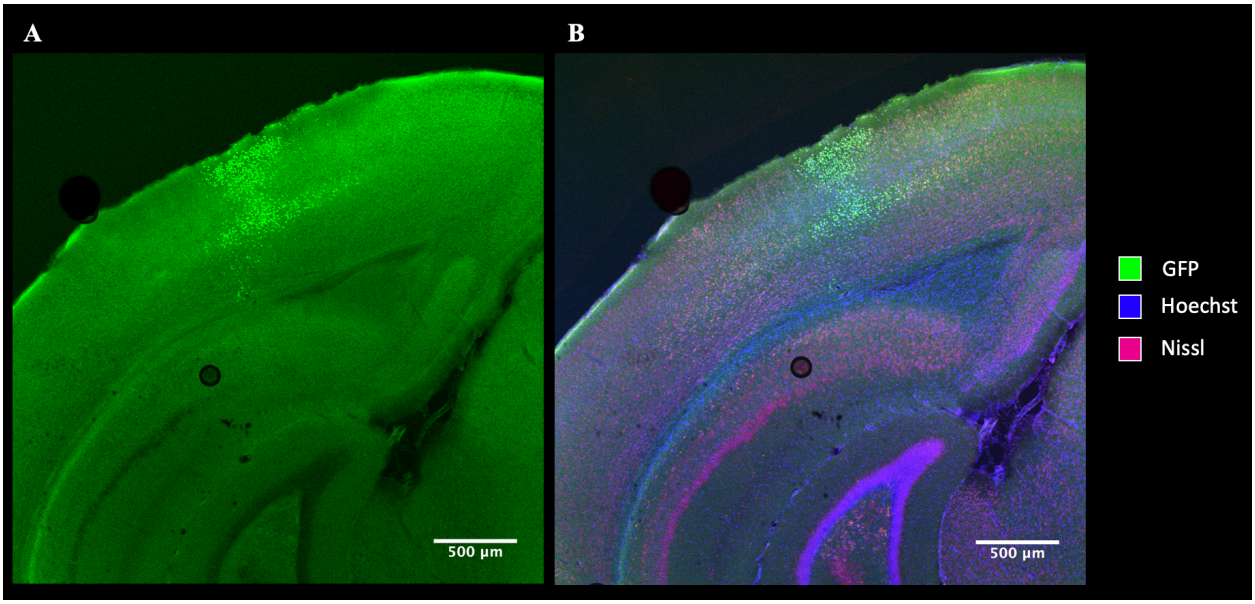

Figure 10: Virally induced Cre-GFP expression in CaMKII-expressing cells was sparse and restricted to the primary visual cortex of injected mice. (**A**) GFP expression (green) in mice injected with AAV8-CaMKII-Cre-GFP in V1 was low and detectable in multiple cortical layers of V1 (L2/3 and L5) by confocal microscopy. The surrounding cerebral tissue also appears green likely due to the confocal microscope's high sensor sensitivity and low signal-to-noise. (**B**) Overlay of **Fig. 10A** with GFP, Hoechst (blue, DNA, 1:10,000 dilution), and Nissl (red, neuronal cell bodies, 1:100 dilution).

To qualitatively determine the efficacy of Cre-mediated recombination in V1, we injected AAV8 expressing Cre recombinase and GFP under the control of the CaMKII promoter in V1 of LoxP-*Grin2b*-LoxP mice and visualized brain tissue via confocal microscopy. We observed

overall weaker GFP expression in cells of layers 2/3 and 5 of V1 and within some of the surrounding tissues (**Fig. 10**). We noted that surrounding neural tissue also had high background autofluorescence, as we compensated for weak GFP expression by overexposing the image. Visually, the level of fluorescence observed was less than that observed in **Fig. 9**, suggesting that either the efficiency of the AAV8 injected into our experimental group was poor or the Cre-mediated recombination triggered a loss of infected cells. As Cre-mediated recombination is highly efficient, V1 neurons that did express GFP, and therefore, Cre, were assumed to have also undergone Cre-mediated recombination.

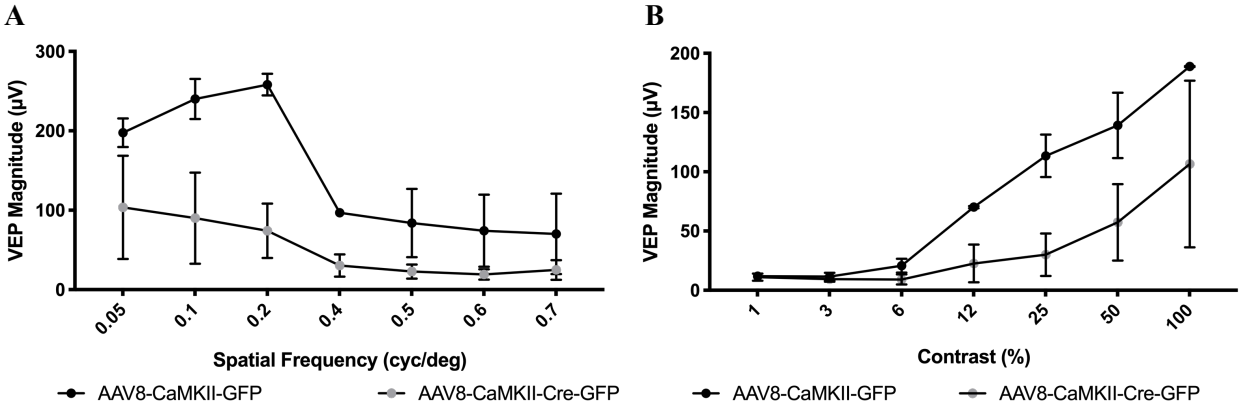

Figure 11: Spatial acuity and contrast sensitivity are mostly preserved in NR2B KO mice relative to control animals. Control mice injected with AAV8-CaMKII-GFP (n = 2) and NR2B KO mice injected with AAV8-CaMKII-Cre-GFP (n = 3) were implanted with electrodes bilaterally in layer 4 of binocular V1 to record electrical activity and a headpost for head stabilization. Following recovery, mice were presented with a grey screen for 2 days to acclimatize mice to the recording rig. (**A**) Head-fixed control (n = 2) and NR2B KO mice (n = 3) were exposed to a 2 Hz phase-reversing, full-field, 100% contrast, 15˚ sinusoidal grating stimulus presented across a range of spatial frequencies (0.05, 0.1, 0.2, 0.4, 0.5, 0.6, 0.7 cycle/degree) (50 phase reversals over 3 blocks). Control and NR2B KO mice are able to distinguish between visual stimuli at different frequencies, and as frequency increases, VEP magnitude decreases (two-way repeated-measures ANOVA, $F_{1.218,3.653} = 8.233$, $p = 0.0488$ for spatial frequency effects). (**B**) Head-fixed control (n = 2) and NR2B KO mice (n = 3) were exposed to a 2 Hz phase-reversing, full-field, 0.05 cycle/degree, 165˚ sinusoidal grating stimulus presented across a range of contrasts (1, 3, 6, 12, 25, 50, 100%) (50 phase reversals over three blocks). Control and NR2B mice are able to distinguish between visual stimuli at different contrasts, and as contrast increases, VEP magnitude increases (two-way repeated-measures ANOVA, $F_{1.165,3.496} = 10.12$, $p = 0.0392$ for contrast effects). Error bars in all graphs represent SEM.

As manipulations of V1 can cause neurological damage that may affect physiological function, we assessed visual acuity and contrast sensitivity in N2RB KO (n = 3) and control mice (n = 2) by measuring VEP magnitudes elicited in layer 4 of binocular V1 during exposure to a 2 Hz phase-reversing, full-field, 100% contrast, sinusoidal grating stimulus across a range of spatial frequencies (0.05-0.7 cycle/degree) and contrasts (1-100%) (50 phase reversals over three blocks). Overall, VEP magnitudes in both NR2B KO and control mice decreased with increasing spatial frequency (**Fig. 11A**; two-way repeated-measures ANOVA, $F_{1.218,3.653} = 8.233$, $p = 0.0488$ for the main effect of spatial frequency), suggesting that the animals were less able to resolve finer details. It is worth mentioning, however, that individual differences in VEP among different frequencies were not statistically significant when analyzed via Sidak's multiple comparison test *post-hoc*, likely a result of the small sample size and Sidak's correction for multiple comparisons. There were no statistically significant differences in VEP magnitudes measured in NR2B KO and control mice (two-way repeated-measures ANOVA, $F_{1,3} = 6.369$, $p = 0.0859$ for the main effect of genotype; two-way repeated-measures ANOVA, $F_{6,18} = 1.724$, $p = 0.1726$ for the interaction of genotype × spatial frequency). Similarly, VEP magnitudes in both NR2B KO and control mice increased with increasing stimulation contrast (**Fig. 11B**; two-way repeated-measures ANOVA, $F_{1.165,3.496} = 10.12$, $p = 0.0392$ for main effect of contrast), indicating that both groups of mice were able to distinguish between different contrasts, although it may be statistically inappropriate to compare groups with such small sample sizes. Again, it is important to note that individual differences in VEP among different contrasts were not statistically significant when analyzed via Sidak's multiple comparison test *post-hoc*. There were no statistically significant differences in VEP magnitudes measured in NR2B KO and control mice (two-way repeated-measures ANOVA, $F_{1,3} = 2.638$, $p = 0.2028$ for the main effect of genotype; two-way repeated-measures ANOVA,

$F_{6,18} = 1.422$, $p = 0.2605$ for the interaction of genotype × contrast). Taken together, our data demonstrates that NR2B KO mice exhibit sensitivity to spatial acuity and contrast, but a trend towards overall smaller VEP magnitudes. As a result, we cannot definitively rule out abnormal vision and visual processing in V1.

In order to determine the role of NR2B in SRP and OSH, after injection with either AAV8-CaMKII-Cre-GFP (n = 3) or control AAV8-CaMKII-GFP (n = 2) into binocular V1, we subjected *Grin2b*$^{fl/fl}$ mice to a visual stimulation protocol known to elicit SRP and OSH. SRP and OSH were measured via electrodes bilaterally implanted in layer 4 of binocular V1 and piezoelectric sensors placed under the forepaws, respectively (**Fig. 12A**). Although it is statistically inappropriate to compare groups with such small sample sizes, as we cannot properly conduct tests for normality and homogeneity of variance, we nevertheless performed two-way repeated-measures ANOVA to compare the effects of genotype and time. In control animals, VEP magnitudes appeared to increase briefly from day 1-3 with further exposure to a 2 Hz phase-reversing, full-field, 0.05 cycle/degree, 100% contrast, 45˚ sinusoidal grating stimulus (100 phase reversals) before plateauing and decreasing from day 4-6, though differences in VEP magnitudes measured daily are not statistically significant (**Fig. 12B**) (two-way repeated-measures ANOVA, $F_{1.533,4.600} = 2.609$, $p = 0.1751$ for the main effect of treatment day; two-way repeated-measures ANOVA, $F_{5,15} = 1.239$, $p = 0.3397$ for the interaction of genotype × treatment day), likely reflecting the small sample size. Similarly, VEP magnitudes measured in NR2B KO animals remained relatively constant from day 1-6 (**Fig. 12B**). Although the measured differences were not statistically significant, we noted a visible difference in overall VEP magnitude between control and NR2B KO mice, with the former exhibiting larger VEP magnitudes than the latter (two-way repeated-measures ANOVA, $F_{1,3} = 8.212$, $p = 0.0643$ for the main effect of genotype). Furthermore, we did

not observe any statistically significant changes in VEP magnitudes when control and NR2B KO mice were exposed to novel stimuli on day 7 (**Fig. 12C**) (two-way repeated-measures ANOVA, $F_{1,3} = 3.380$, $p = 0.1633$ for the main effect of genotype; $F_{1,3} = 4.043$, $p = 0.1379$ for the main effect of stimulus). Taken together, these preliminary data cannot definitively characterize the role of NR2B in the acquisition of SRP in p56-66 C57BL/6 mice, since our observations may be confounded by high variance stemming from small sample sizes and methodological challenges.

In addition to SRP, in NR2B KO (n = 3) and control (n = 2) mice we also examined OSH—a reduction in a reflexive behavior—that co-occurs with SRP and relies on NMDA receptor activity in V1 (Cooke et al., 2015). Using the same six-day visual stimulation protocol (**Fig. 12A**), we measured vidget magnitudes to the onset of each block of stimuli each day, in both NR2B KO mice and control mice, via a piezoelectric sensor placed under the forepaws. Vidget magnitudes were normalized to baseline forepaw movements recorded during the 2 s prior to exposure to visual stimuli. In both NR2B KO and control mice, we did not observe statistically significant changes to vidget magnitude from day 1-6, and vidget magnitude remained relatively constant (**Fig. 12D**) (two-way repeated-measures ANOVA, $F_{1,3} = 0.01$, $p = 0.9059$ for the main effect of genotype; $F_{2.353,7.059} = 0.6676$, $p = 0.5653$ for the main effect of treatment day). Moreover, we did not observe any statistically significant changes in vidget magnitudes when control and NR2B KO mice were exposed to a novel stimulus on day 7 (**Fig. 12E**) (two-way repeated-measures ANOVA, $F_{1,3} = 0.89$, $p = 0.4149$ for the main effect of genotype; $F_{1,3} = 0.16$, $p = 0.7158$ for the main effect of treatment day). From our prior experience, vidget magnitudes decrease with increasing familiarity to visual stimuli and spontaneously increase when mice are exposed to a subsequent novel stimulus.

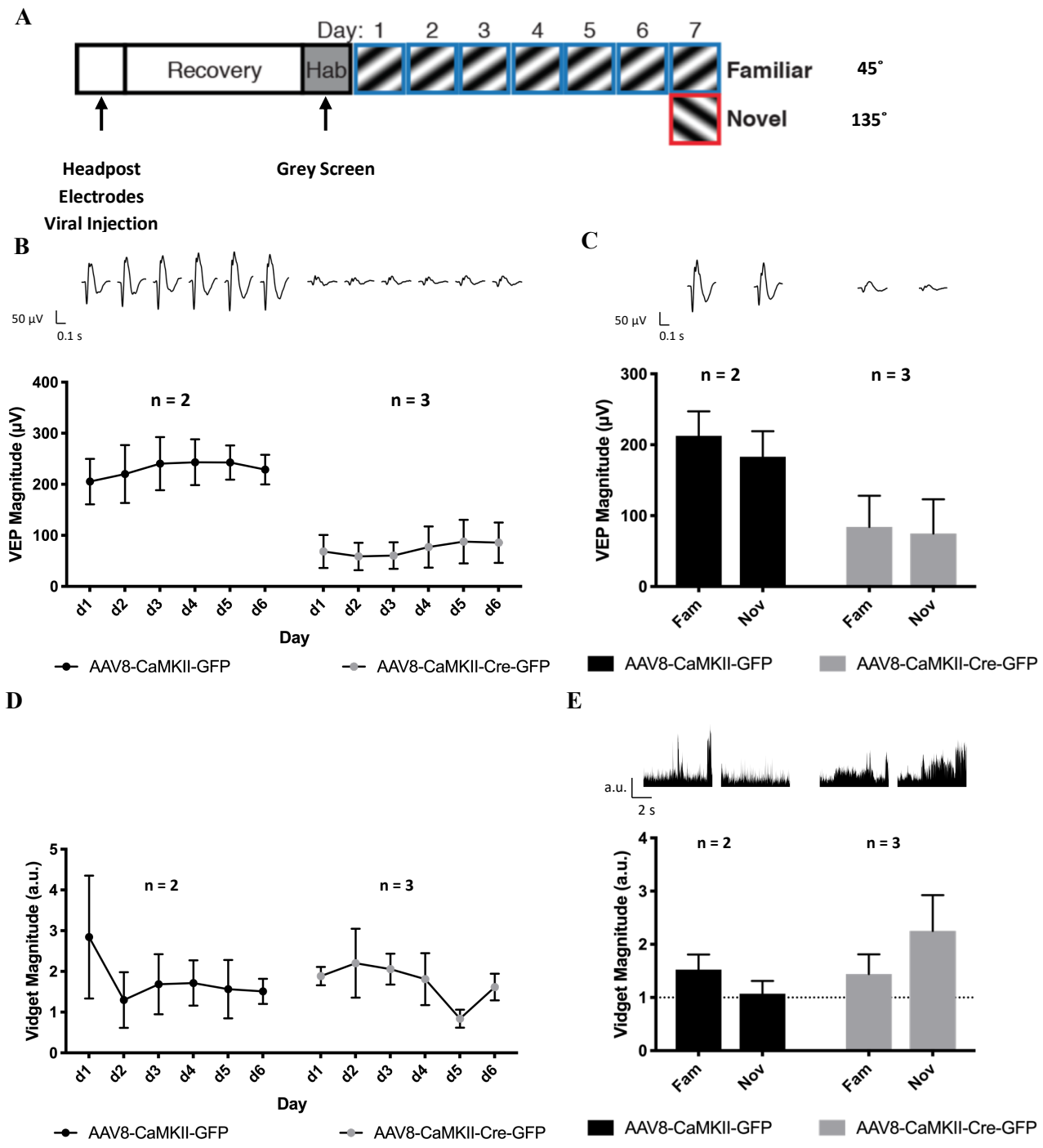

Figure 12: Loss of NR2B may reduce baseline VEP magnitude. (**A**) Control mice injected with AAV8-CaMKII-GFP (n = 2) and NR2B KO mice injected with AAV8-CaMKII-Cre-GFP (n = 3) were implanted with electrodes and headpost and acclimatized as described previously. Piezoelectric sensors were also placed under the forepaws to measure movement. For the next six days, a 45˚ sinusoidal grating stimulus was presented on the monitor. On day 7, both the familiar 45˚ stimulus and a novel 135˚ stimulus were presented in interleaved order to assess SRP and OSH. (**B**) VEP magnitudes remained relatively constant for control (n = 2) and NR2B KO (n = 3)

exposed to six days of a 45˚ sinusoidal grating stimulus, VEP magnitudes do not differ significantly between the two groups. Average VEP waveforms are displayed above the graph. Vertical scale bar represents 50 μV; horizontal scale bar represents 0.1 s. (**C**) VEP magnitudes do not differ significantly when control (n = 2) or NR2B KO mice (n = 3) are shown familiar and novel stimuli on day 7. Average VEP waveforms are also provided above the graph. Vertical scale bar represents 50 μV; horizontal scale bar represents 0.1 s. (**D**) Vidget magnitudes remained relative constant in control mice (n = 2) and NR2B KO mice (n = 3) exposed to six days of a 45˚ sinusoidal grating stimulus and did not differ significantly between the two groups. (**E**) Vidget magnitudes do not differ significantly when control (n = 2) or NR2B KO mice (n = 3) are shown familiar and novel stimuli on day 7. Average vidget waveforms are also provided above the graph. Vertical scale bar represents 1 a.u.; horizontal scale bar represents 2 s. Average vidget magnitudes were normalized to baseline forepaw movements obtained during the 2 s prior to visual stimuli (dotted line). All full-field phase-reversing stimuli were presented at 2 Hz, 0.05 cycle/degree, 100% contrast, and 100 phase reversals over 5 blocks. Statistical analysis was performed via two-way repeated-measures ANOVA. Error bars in all graphs represent SEM.

4.3 Effect of NR2B pharmacological inhibition on the acquisition of SRP and OSH

4.4.1 Effect of NR2B inhibition via CP-101,606 on SRP and OSH

Since we encountered several challenges with the viral injection approach to knockout NR2B, including low expression of AAV8 in layer 4 of binocular V1 (**Fig. 10**) and apparently poor VEP potentiation in control animals (**Fig. 12B and 12C**), we switched to a pharmacological approach to inhibit NR2B in order to delineate the role of NR2B in SRP and OSH (**Fig. 13A**). Wild-type mice were initially presented with a 2 Hz, 0.05 cycle/degree, 100% contrast, 135˚ sinusoidal grating stimulus (100 phase reversals over five blocks) before being subjected to intraperitoneal injections of either 75% v/v DMSO (vehicle control) (n = 5) or 10 mg/kg CP-101,606 (n = 4). One hour following injection, mice were presented with a 45˚ sinusoidal grating stimulus (five blocks). On day 3, mice in both treatment groups were presented with five blocks of 135˚ ("pre-drug familiar"), 45˚ ("post-drug familiar"), and 75˚ ("post-drug novel") sinusoidal grating stimuli. On day 7, all mice were presented with four blocks of the pre-drug familiar 135˚, post-drug familiar 45˚, post-drug familiar 75˚, and novel 105˚ sinusoidal grating stimuli. VEP and vidget magnitudes

were measured via bilaterally implanted electrodes in layer 4 of binocular V1 and piezoelectric sensors placed underneath the forepaws, respectively.

In vehicle-treated mice, VEP magnitudes elicited by the pre-drug familiar 135˚ stimulus was lower than the VEP magnitude elicited by the post-drug familiar 45˚ stimulus, indicating that DMSO may have a baseline effect on normal physiology (**Fig. 13B**). VEP magnitudes elicited by the pre-drug familiar 135˚ stimulus appeared to increase from day 1-3 and levelled off between day 3-7 (**Fig. 13B**). The initial increase in VEP magnitude, though not statistically significant, appears to reflect SRP and suggests successful acquisition and consolidation of cortical plasticity. Interestingly, in the same group of mice, VEP magnitudes elicited by the post-drug familiar 45˚ stimulus appeared to remain constant between day 1-3 and seemed to only increase from day 3-7 (**Fig. 13B**). The constancy of VEP magnitudes during this initial three-day period suggests that potentiation may not have occurred, as a result of DMSO. Following washout of DMSO, SRP could apparently be induced for this previously unpotentiated response by day 3, as revealed by the increase in VEP magnitudes to the post-drug 45˚ stimulus on day 7. VEP magnitudes corresponding to the post-drug familiar 75˚ stimulus also increased from day 3-7, suggesting normal potentiation and SRP acquisition. Taken together, these data suggest that DMSO alone occludes the initial acquisition, but not the consolidation, of visual memory.

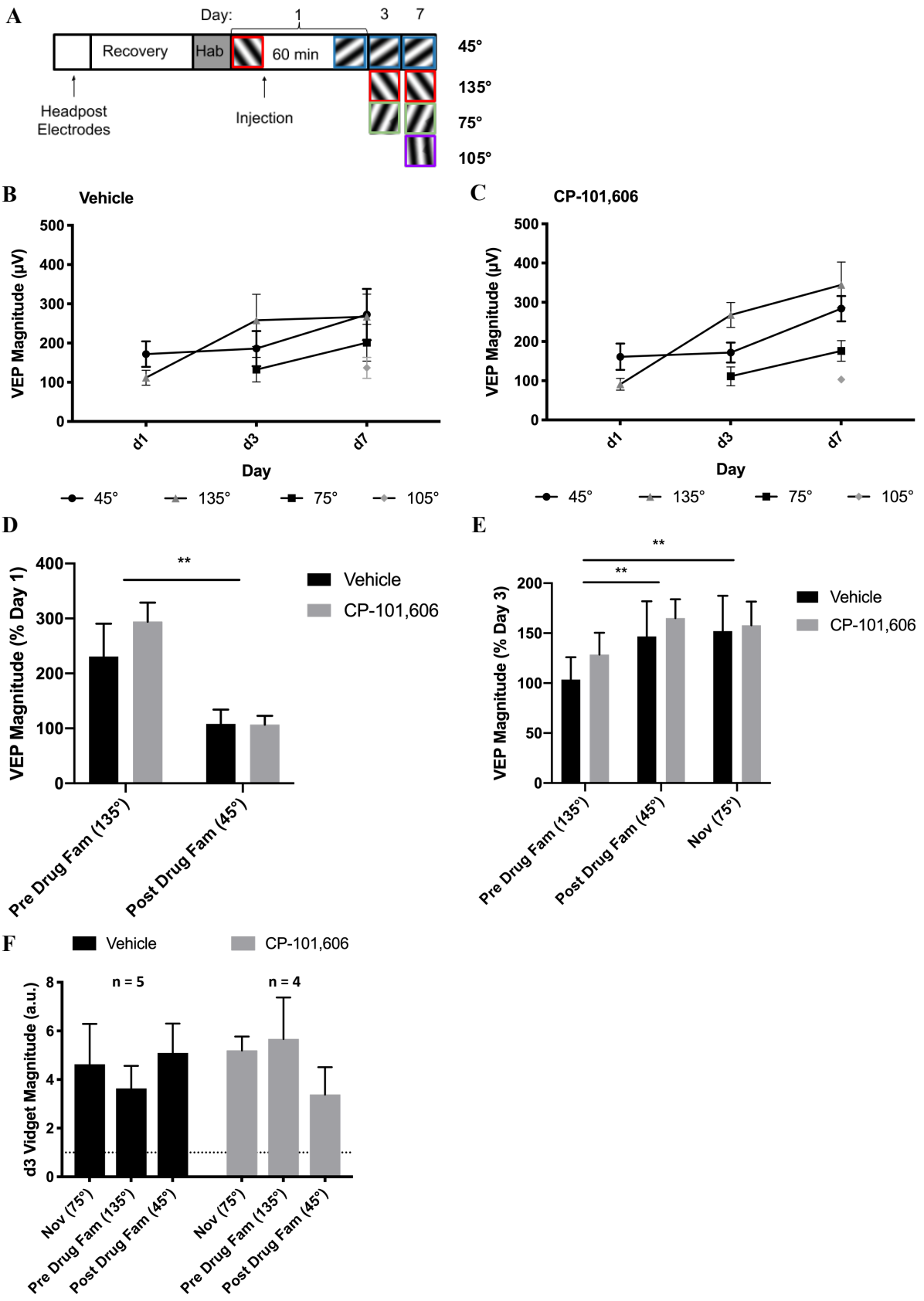
A
Day:
1
3
7
Recovery
Hab
60 min
45°
135°
75°
105°
Headpost
Electrodes
Injection
B
Vehicle
VEP Magnitude (µV)
Day
d1
d3
d7
45°
135°
75°
105°
C
CP-101,606
VEP Magnitude (µV)
Day
d1
d3
d7
45°
135°
75°
105°
D
VEP Magnitude (% Day 1)
**
Vehicle
CP-101,606
Pre Drug Fam (135°)
Post Drug Fam (45°)
E
VEP Magnitude (% Day 3)
**
**
Vehicle
CP-101,606
Pre Drug Fam (135°)
Post Drug Fam (45°)
Nov (75°)
F
Vehicle
CP-101,606
d3 Vidget Magnitude (a.u.)
n = 5
n = 4
Nov (75°)
Pre Drug Fam (135°)
Post Drug Fam (45°)
Nov (75°)
Pre Drug Fam (135°)
Post Drug Fam (45°)

Figure 13: High concentration DMSO vehicle, not CP-101,606, likely occludes the acquisition, but not consolidation, of visual memory. (**A**) Mice were implanted with electrodes and headpost and acclimatized mice as described previously. Mice were then presented with a 135˚ sinusoidal grating stimulus (5 blocks) on day 1. On the same day, mice were injected intraperitoneally with either vehicle (75% v/v DMSO) (n = 5) or CP-101,606 (10 mg/kg) (n = 4) and exposed to a second 45˚ sinusoidal grating stimulus (5 blocks) one hour after injection. On day 3, all mice were presented with the pre-drug familiar 135˚ stimulus, post-drug familiar 45˚ stimulus, and a novel 75˚ stimulus (5 blocks per stimulus) to assess SRP and OSH. On day 7, all mice were presented with the pre-drug familiar 135˚ stimulus, post-drug familiar 45˚ stimulus, the previously novel 75˚ stimulus, and a true novel 105˚ stimulus (4 blocks per stimulus) to reassess SRP retention and acquisition. VEP magnitudes were measured on day 1, 3, and 7. (**B**) and **(C)** VEP magnitudes elicited by different orientations pre- and post-drug injection on day 1, 3, and 7 suggest DMSO inhibits acquisition, but not consolidation, of visual memory in vehicle-treated mice (n = 5) and CP-101,606-treated mice (n = 4), respectively. (**D**) Day 3 VEP magnitudes were normalized to day 1 VEP magnitudes (% of Day 1) in vehicle (n = 5) and CP-101,606-treated animals (n = 4). There is greater evidence of VEP potentiation elicited by the pre-drug familiar 135˚ stimulus than the post-drug familiar 45˚ stimulus across both groups (two-way repeated-measures ANOVA: $F_{1,7} = 26.2$, $p = 0.0014$ for stimulus effects). (**E**) Day 7 VEP magnitudes were normalized to day 3 VEP magnitudes (% of Day 3) in vehicle (n = 5) and CP-101,606-treated animals (n = 4). Across both groups, the increase in VEP magnitudes elicited by the pre-drug familiar 135˚ stimulus was less than those elicited by both the post-drug familiar 45˚ stimulus and the post-drug familiar 75˚ stimulus (two-way repeated-measures ANOVA, $F_{2,14} = 11.26$, $p = 0.0012$ for stimulus effects). (**F**) There were no statistically significant differences between recorded vidget magnitudes on day 3 in all stimulus conditions and treatment groups. Dotted line indicates mean baseline forepaw movement recorded during the 2 s before visual stimulation. All full-field phase-reversing stimuli were presented at 2 Hz, 0.05 cycle/degree, 100 phase reversals per block, and 100% contrast. Error bars in all graphs represent SEM. ** represents a statistically significant comparison with $p \leq 0.01$.

Interestingly, the same patterns of potentiation were observed in all stimulation conditions in mice treated with 10 mg/kg of known selective NR2B antagonist CP-101,606 (**Fig. 13C**). Given the baseline effects of the DMSO vehicle on VEP magnitudes observed in vehicle control animals, the effects of CP-101,606 were not immediately clear. Irrespective of treatment group, VEP magnitudes elicited by the post-drug 45˚ visual stimulus were greater than the VEP magnitude elicited by the pre-drug 135˚ visual stimulus (two-way repeated-measures ANOVA, $F_{1,7} = 6.430$, $p = 0.0389$ for stimulus effects) on day 1. On day 3, the VEP magnitudes elicited by the pre-drug familiar 135˚, post-drug familiar 45˚, and post-drug novel 75˚ visual stimuli differed significantly (two-way repeated-measures ANOVA, $F_{2,14} = 12.62$, $p = 0.0007$ for stimulus effects). A closer

statistical examination via Sidak's multiple comparison test *post-hoc* revealed that the pre-drug familiar 135˚stimulus potentiated VEPs to a greater extent than the post-drug familiar 45˚ stimulus by day 3 (adj. $p = 0.0299$); the pre-drug familiar 135˚ stimulus also elicited larger VEPs than the post-drug familiar 75˚ stimuli (adj. $p = 0.0006$) on day 3. On day 7, the VEP magnitudes elicited by the pre-drug familiar 135˚, post-drug familiar 45˚, and post-drug familiar 75˚ visual stimuli differed significantly (two-way repeated-measures ANOVA, $F_{3,21} = 24.24$, $p < 0.0001$ for stimulus effects). Again, Sidak's multiple comparison test revealed that the pre-drug familiar 135˚ stimulus potentiated VEPs to a greater extent than the post-drug familiar 75˚ stimulus (adj. $p = 0.0006$) and elicited larger VEPs than the post-drug novel 105˚ stimulus (adj. $p < 0.0001$). The post-drug familiar 45˚ stimulus also potentiated VEPs to a greater extent than the post-drug familiar 75˚ stimulus (adj. $p = 0.0083$) and elicited larger VEPs than the post-drug post-drug familiar 105˚ stimulus (adj. $p < 0.0001$) on day 7.

In order to closer examine the effect of pharmacological treatment on potentiation, we normalized day 3 VEP magnitudes to day 1 VEP magnitudes to determine the change in VEP magnitude in vehicle-treated and CP-101,606-treated mice exposed to the pre-drug familiar 135˚ and post-drug familiar 45˚ stimuli (**Fig. 13D**). While no statistically significant differences were observed between vehicle-treated mice and CP-101,606-treated mice, suggesting that CP-101,606 has no observable effect on SRP (two-way repeated-measures ANOVA, $F_{1,7} = 0.39$, $p = 0.5476$ for drug effects), we did observe significant differences in VEP magnitudes between mice exposed to the pre-drug familiar 135˚ and post-drug familiar 45˚ stimuli (two-way repeated-measures ANOVA: $F_{1,7} = 26.2$, $p = 0.0014$ for stimulus effects). Similarly, we normalized day 7 VEP magnitudes to day 3 VEP magnitudes in vehicle-treated and CP-101,606-treated mice exposed to the pre-drug familiar 135˚, post-drug familiar 45˚, and post-drug novel 75˚ stimuli (**Fig. 13E**).

Again, while no statistically significant differences were observed between vehicle-treated and CP-101,606-treated mice (two-way repeated-measures ANOVA, $F_{1,7} = 0.1792$, $p = 0.6848$ for drug effects), suggesting that CP-101,606 has no observable effect on SRP, we did observe significant differences in VEP potentiation between mice exposed to the pre-drug familiar 135˚, post-drug familiar 45˚, and post-drug novel 75˚ stimuli (two-way repeated-measures ANOVA, $F_{2,14} = 11.26$, $p = 0.0012$ for stimulus effects). Sidak's multiple comparison test revealed that the pre-drug familiar 135˚ stimulus potentiated VEPs to a greater extent than the post-drug familiar 45˚ stimulus (adj. $p = 0.0029$) and the post-drug novel 75˚ stimulus (adj. 0.0035). Taken together, these data support our conclusion that DMSO occludes the acquisition of SRP as visual stimuli presented before DMSO-treatment are able to potentiate VEPs, in contrast to stimuli presented immediately after DMSO-treatment.

Given that OSH and SRP emerge in parallel, we also measured vidget magnitudes in all mice on day 3. After normalizing day 3 vidget magnitudes to baseline forepaw movements recorded 2 s prior to visual stimulation, we did not observe any statistically significant differences between vehicle-treated and CP-101,606-treated mice and between mice presented with pre-drug familiar 135˚, post-drug familiar 45˚, and post-drug novel 75˚ stimuli (two-way repeated-measures ANOVA, $F_{1,7} = 0.06685$, $p = 0.8034$ for drug effects; $F_{1.778,12.45} = 0.1519$, $p = 0.8374$ for stimulus effects).

4.4.2 Effect of NR2B inhibition via Ro 25-6981 on SRP and OSH

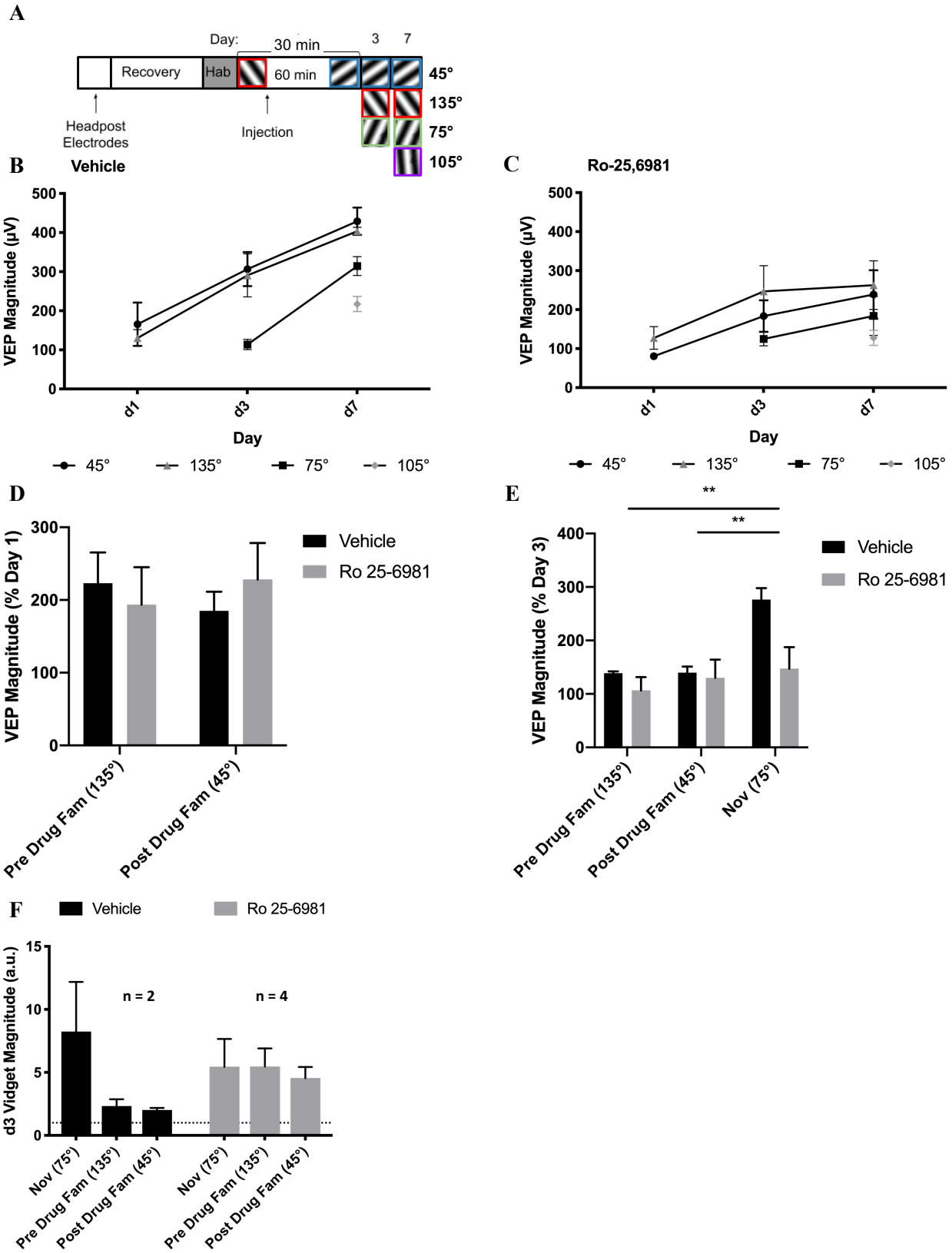

Figure 14: Selective NR2B antagonist Ro 25-6981 does not appear to attenuate SRP or OSH. (**A**) Mice were implanted with electrodes and headpost and acclimatized as described previously. Mice were then presented with a 135˚ sinusoidal grating stimulus (5 blocks) on day 1. On the same day, mice were injected intraperitoneally with either vehicle (saline) (n = 2) or Ro 25-6981 (10 mg/kg) (n = 4) and exposed to a second 45˚ sinusoidal grating stimulus (5 blocks) 30 min after injection. From day 3 onwards, mice were subjected to the same visual stimulation protocol used in the CP-101,606 NR2B inhibition experiment. (**B**) and **(C)** VEP magnitudes elicited by familiar orientations on day 1, 3, and 7 appeared to increase in vehicle-treated (n = 2) and Ro 25-6981-treated mice (n = 4). (**D**) Day 3 VEP magnitudes were normalized to day 1 VEP magnitudes (% of Day 1) in vehicle (n = 2) and Ro 25-6981-treated animals (n = 4). No statistically significant differences were observed between pre-drug familiar 135˚ stimulus and post-drug familiar 45˚ stimulus or between vehicle and Ro 25-6981-treated animals. (**E**) Day 7 VEP magnitudes were normalized to day 3 VEP magnitudes (% of Day 3) in vehicle and Ro 25-6981-treated animals. The increase in VEP magnitudes elicited by the pre-drug familiar 135˚ stimulus or the post-drug familiar 45˚ stimulus were smaller than those elicited by the post-drug familiar 75˚ stimulus across both groups (two-way ANOVA: $F_{2,8} = 20.0$, $p = 0.0008$ for stimulus effects). (**F**) There were no statistically significant differences between recorded vidget magnitudes on day 3 in all stimulus conditions and treatment groups. Dotted line indicates mean baseline forepaw movement recorded during the 2 s before visual stimulation. All full-field phase-reversing stimuli were presented at 2 Hz, 0.05 cycle/degree, 100 phase reversals per block, and 100% contrast. Error bars in all graphs represent SEM. ** represents a statistically significant comparison with $p \leq 0.01$.

Given a potential baseline effect of DMSO-containing vehicle on SRP, which confounded our observations of the effect of CP-101,606 on SRP and OSH, we investigated replacing CP-101,606 with a second selective NR2B antagonist Ro 25-6981 that is dissolvable in saline (**Fig. 14A**), thereby obviating the use of DMSO. Wild-type mice were initially presented with a 2 Hz, 0.05 cycle/degree, 100% contrast, 135˚ sinusoidal grating stimulus (100 phase reversals over five blocks) before being subjected to intraperitoneal injections of either saline (vehicle control) (n = 2) or 10 mg/kg Ro 25-6981 (n = 4). Thirty minutes following injection, mice were presented with a 45˚ sinusoidal grating stimulus (five blocks). From day 3 onward, mice were subjected to the same visual stimulation protocol used in the CP-101,606 NR2B inhibition experiment.

In vehicle-treated mice (**Fig. 14B**), the pre-drug familiar 135˚ stimulus appeared to increase from day 1-7, suggesting the occurrence of SRP and the acquisition and consolidation of visual memory. VEP magnitudes elicited by the post-drug familiar 45˚ stimulus also appeared to increase

from day 1-3 and day 3-7, again indicating the occurrence of SRP. There were no statistically significant differences between VEP magnitudes measured in either stimulation condition. Stated otherwise, the occlusion of visual memory acquisition likely observed following DMSO treatment was not seen here. VEP magnitudes elicited by the post-drug familiar 75˚ stimulus also appeared to increase from day 3-7 (**Fig. 14B**).

In Ro 25-6981-treated mice (**Fig. 14C**), VEP magnitudes elicited by the pre-drug familiar 135˚ stimulus appeared to increase from day 1-3 and then plateaued from day 3-7. This initial increase suggests the likely acquisition and consolidation of SRP, as seen in the vehicle-control mice, despite treatment with a selective NR2B antagonist. Similarly, VEP magnitudes elicited by the post-drug familiar 45˚ stimulus appeared to increase gradually from day 1-7, and VEP magnitudes elicited by the post-drug familiar 75˚ stimulus appeared to increase from day 3-7 (**Fig. 14C**). No statistically significant differences were observed between vehicle-treated and Ro 25-6981-treated animals in any of the visual stimulation conditions on day 1 (two-way repeated-measures ANOVA, $F_{1,4} = 1.942$, $p = 0.2359$ for drug effects), day 3 (two-way repeated-measures ANOVA, $F_{1,4} = 0.7221$, $p = 0.4433$ for drug effects), or day 7 (two-way repeated-measures ANOVA, $F_{1,4} = 3.962$, $p = 0.1174$ for drug effects). Irrespective of treatment group, VEP magnitudes elicited by the pre-drug familiar 135˚, post-drug familiar 45˚, and post-drug novel 75˚ visual stimuli differed significantly on day 3 (two-way ANOVA: $F_{2,8} = 10.82$, $P = 0.0053$ for stimulus effects), though VEP magnitudes elicited by the pre-drug familiar 135˚ and post-drug familiar 45˚ stimuli did not differ significantly on day 1 (two-way repeated-measures ANOVA, $F_{1,4} = 0.05092$, $p = 0.8325$ for stimulus effects). Sidak's multiple comparison test revealed that the pre-drug familiar 135˚ stimulus elicited larger VEP magnitudes than the post-drug familiar 75˚ stimulus (adj. $p = 0.0075$) and post-drug familiar 45˚ stimulus elicited larger VEP magnitudes post-drug familiar 75˚ stimuli

(adj. $p = 0.0196$) on day 3. Similarly, day 7 VEP magnitudes elicited by the pre-drug familiar 135˚, post-drug familiar 45˚, post-drug familiar 75˚, and post-drug novel 105˚ visual stimuli differed significantly (two-way ANOVA: $F_{3,12} = 12.97$, $P = 0.0004$). Again, Sidak's multiple comparison test revealed that the pre-drug familiar 135˚ stimulus elicited larger VEP magnitudes than the post-drug novel 105˚ stimulus (adj. $p = 0.0012$) and the post-drug familiar 45˚ stimulus elicited larger VEP magnitudes than the post-drug novel 105˚ stimulus (adj. $p = 0.0011$).

To explore changes in VEP magnitudes between vehicle-treated and Ro 25-6981-treated mice exposed to the pre-drug familiar 135˚ and post-drug familiar 45˚ stimuli, we normalized day 3 VEP magnitudes to day 1 VEP magnitudes (**Fig. 14D**). No statistically significant differences were observed between vehicle-treated mice and Ro 25-6981-treated mice (two-way repeated-measures ANOVA, $F_{1,4} = 0.008359$, $p = 0.9315$ for drug effects), which support our prior observation that Ro 25-6981 has no observable effect on SRP, and between mice exposed to the pre-drug familiar 135˚ and post-drug familiar 45˚ stimuli (two-way repeated-measures ANOVA, $F_{1,4} = 0.005116$, $p = 0.9464$ for stimulus effects). We also normalized day 7 VEP magnitudes to day 3 VEP magnitudes in vehicle-treated and Ro 25-6981-treated mice exposed to the pre-drug familiar 135˚, post-drug familiar 45˚, and post-drug novel 75˚ stimuli (**Fig. 14E**). Interestingly, while no statistically significant differences were observed between vehicle-treated and Ro 25-6981-treated mice (two-way repeated-measures ANOVA, $F_{1,4} = 1.41$, $p = 0.2998$ for drug effects), we saw significant differences in VEP magnitudes between mice exposed to the pre-drug familiar 135˚, post-drug familiar 45˚, and post-drug novel 75˚ stimuli (two-way ANOVA, $F_{2,8} = 20.0$, $p = 0.0008$ for stimulus effects; $F_{2,8} = 8.64$, $p = 0.01$ for stimulus × drug interaction). It is worth noting, however that Sidak's multiple comparison test failed to identify any statistically significant differences in day 7 VEP magnitudes between stimulation conditions, likely due to Sidak's

correction for multiple comparisons and the small control sample size. Taken together, these data suggest that despite its role in the selective inhibition of NR2B, Ro 25-6981 likely does not affect SRP acquisition or consolidation, although it does appear to influence the potentiation of VEPs to novel stimuli presented 48 hours following injection. This could reflect some type of compensatory homeostatic shift in NMDA receptor expression or composition.

As before, we also measured vidget magnitudes in all mice on day 3 to examine the effects of Ro 25-6981 on OSH. After normalizing day 3 vidget magnitudes to baseline forepaw movements recorded 2 s prior to visual stimulation, we did not observe any statistically significant differences between vehicle-treated and Ro 25-6981-treated mice (two-way repeated-measures ANOVA, $F_{1,4} = 1.41$, $p = 0.2998$ for drug effects) and between mice presented with pre-drug familiar 135˚, post-drug familiar 45˚, and post-drug novel 75˚ stimuli (two-way repeated-measures ANOVA, $F_{1,4} = 1.41$, $p = 0.2998$ for stimulus effects).

5 Discussion

5.1 NMDA receptor subunit composition in V1 neurons does not change during SRP

The goals of this project were two-fold: to describe how the subunit composition of NMDA receptors expressed in neurons of V1 change during the acquisition of visual memory, and to elucidate the role of NMDA receptor subunit NR2B in correlates of recognition memory, SRP and OSH. We were unable to observe any statistically significant changes to the NR2A/NR2B ratio in mice that underwent a visual stimulation protocol previously reported to elicit SRP based on protein quantification via Western blot, suggesting that at least during the 6-day time course of our experiment, NMDA receptor subunit expression does not change at the level of non-fractionated homogenates. Rapid NMDA receptor subunit composition changes have previously been reported in 1-6-week-old dark-reared rats upon light exposure, suggesting a rapid change in NMDA receptor biochemistry with increasing visual experience (Quinlan et al., 1999). It is worth noting that in these past reports, animals undergo substantive changes in visual experience, from never having been exposed to their visual environments to full stimulation of V1 via new visual inputs, perhaps explaining the significant alterations in NMDA receptor composition. In contrast to our current work, while mice are able to recognize a sinusoidal grating 45˚ stimulus presented over the course of 6 days, the magnitude of the stimulus may not be sufficient to generate detectable changes to the NR2A/NR2B ratio.

Interestingly, despite the absence of significant differences between the different stimulation conditions, there appears to be a tendency towards increased NR2B and NR2A expression in all mice that were presented with non-grey screen stimuli (sinusoidal grating 45˚ stimulus for a single day or 6 days) with no concordant changes in NR1 expression (**Fig. S1; Fig. S2**). Taken together, these trends suggest that while the total number of NMDA receptors do not change based on the number of obligatory NR1 subunits, visual experience enhances NR2B and NR2A expression

levels. Recognizing that functional NMDA receptors must contain two NR1 subunits and two, variable NR2/3 subunits and that the replacement of NR2B by NR2A occurs during the production of new NMDA receptors only, we propose several explanations for our observations here. First, it is possible that we are unable to appreciate statistically significant changes in NR1 expression given its high baseline expression level. Second, though the focus of our experiment was on NR2A and NR2B, it is possible that NMDA receptors containing other subunits, including NR2C, NR2D, or any of the NR3 subtypes, which play a role in visual memory, may be expressed to replace the existing NR2B-containing NMDA receptors. Finally, the increase in NR2A and NR2B expression reflect a pool of NMDA receptor subunits that have yet to be assembled to form new NMDA receptors or a pool of intact NMDA receptors that have yet to be degraded. This hypothesis suggests a possible time-lag between visual memory acquisition and NMDA receptor subunit exchange. Further experiments are needed to investigate and distinguish between these hypotheses to fully elucidate biochemical changes to NMDA receptors during visual memory acquisition.

With regards to detection sensitivity, it is also important to recognize limitations in our methodology. In addition to a small sample size (n = 5), which may contribute to larger variances in the data and obscure potentially significant findings, our experiment was conducted such that V1 cortical tissue was dissected and homogenized for protein extraction. Since dissection was performed manually, and there are no consistent anatomical markers for boundaries around V1, it is possible that cortical regions other than V1 were also isolated along with V1. Since visual stimulus-dependent changes likely predominantly affect V1, we would not expect there to be changes in NMDA receptor subunit composition outside of V1. As the frontal cortex had been used in previous monocular deprivation experiments in the Bear Lab, this guided our choice in using frontal cortical tissue as a negative control in our experiment. If there were indeed changes

in NMDA receptor composition in V1 during the acquisition of visual memory, the presence of proteins from non-V1 cortical regions may have obscured these changes by diluting the magnitude of the change. Future experiments may be able to eliminate these potential sources of error by increasing sample size to enhance statistical power and by selectively isolating V1 neurons via synaptoneurosome fractionation. Given that NMDA receptor subunits are functional on the synaptic membrane only, future iterations of our experiments may also opt to use specialized techniques, including subcellular fractionation, to isolate plasma membrane proteins for analysis in order to increase the signal-to-noise ratio. It is worth mentioning that relative NR2A, NR2B, NR1, and β-actin levels were quantified using Western blot and software tools to analyze protein immunoblot images. As detection sensitivity is limited by computer algorithms and the resolution of the images generated, which may underreport proteins present at higher concentrations, our ability to accurately quantify proteins may be called into question. Future iterations of this project may seek to use more sophisticated tools to quantify specific proteins, including mass spectrometry or enzyme-linked immunosorbent assay.

5.2 Genetic ablation of NR2B was unable to reveal the role of NR2B in SRP and OSH

In order to delineate the role of NMDA receptor subunit NR2B in SRP and OSH, we selectively deleted *Grin2b* in *Grin2b*$^{fl/fl}$ mice via viral infection with AAV8-CaMKII-Cre-GFP and measured SRP and OSH during visual stimulation four weeks post-infection. Given that there were no statistically significant differences in VEP magnitudes measured within NR2B KO mice and control mice (*Grin2b*$^{fl/fl}$ mice injected with AAV8-CaMKII-GFP) groups or between the two groups, we were unable to determine the role of NR2B in SRP and OSH (**Fig. 12**). A closer examination of the data suggests that there may be a statistically insignificant upward trend in VEP magnitudes and a downward trend in vidget magnitudes in both groups of mice across the 6 days

of visual stimulation, perhaps suggesting the manifestation of SRP and OSH, respectively, and implying that NR2B knockout may not affect the acquisition of visual memory (**Fig. 12**). However, no definitive conclusions can be drawn given that SRP and OSH were not observed as expected from our prior work (Cooke et al., 2015). Visual function (spatial acuity and contrast sensitivity) was preserved in both groups of mice (**Fig. 11**), and VEP waveforms look consistent with previous reports, suggesting no issues with normal electrophysiology in both groups of mice (**Fig. 12B and 12C**) (Cooke et al., 2015; Frenkel et al., 2006). Interestingly, though statistically insignificant, there appears to be a difference between average VEP magnitudes measured in control mice compared to those measured in NR2B KO mice, suggesting that the loss of NR2B decreases responsiveness to visual stimuli. Given that prior research on related NMDA receptor subunit NR2A has demonstrated that a loss of NR2A function enhances synaptic strengthening while diminishing synaptic weakening, leading to increased potentiation in monocular deprivation experiments (Cho et al., 2009; Massey et al., 2004; Philpot et al., 2007), the loss of NR2B may cause the opposite effect, namely the enhancement of synaptic weakening and the inhibition of synaptic strengthening. This theory may potentially be consistent with our findings of reduced VEP magnitudes in NR2B KO mice here. Alternatively, the loss of NR2B may result in the compensatory overexpression of NMDA receptor subunits NR1 and NR2A, leading to a larger number of synaptic NMDA receptors and enhanced potentiation. This hypothesis is supported by prior observations, which demonstrated that the genetic ablation of NR1 or inhibition of NMDA receptors in general both abolished SRP and reduced baseline VEP magnitudes elicited by a novel stimulus. This latter effect mirrors our observations here. We must recognize, however, that there is evidence that may refute our hypothesis. Indeed, selective disruption of NR2A does not lead to the compensatory overexpression of NR1 and NR2B (Philpot et al., 2007). While this finding does

not preclude our hypothesis, future iterations of our experimental approach may opt to examine NR1 and NR2A expression levels following selective NR2B deletion.

There are several potential caveats and alternative explanations for our findings. First, it is important to acknowledge the inconsistent infectivity of AAV8 and its imprecise expression in binocular V1. In AAV8-CaMKII-GFP-infected mice, confocal fluorescence microscopy indicated high levels of infection, as evidenced by the presence of GFP expression in cortical areas outside of lateral V1, including V2 (**Fig. 9**). These control mice also did not exhibit SRP and OSH, which may be attributable to the small sample size (n = 2) (**Fig. 12**) or physiological effects related to AAV8 infection. This latter hypothesis is supported by prior work, which has suggested that AAV8-induced GFP expression is associated with toxicity in rat hippocampal neurons (Klein et al., 2006). The absence of SRP and OSH in our control group is important to address as it may obscure statistically significant differences observed in our NR2B KO group.

On the other hand, confocal fluorescence microscopy indicated that cells within layers 2/3 and 5, but not layers 4 and 6, in binocular V1 expressed AAV8-CaMKII-Cre-GFP and cells outside of V1 also expressed the transgene (**Fig. 10**). The former observation likely suggests that our conditional NR2B knockout was only partially successful, and our findings may be confounded by the mosaic genotype of the mice. In other words, our NR2B KO mice may have a significant proportion of CaMKII-expressing V1 neurons that retain NR2B function, thereby compensating for the small number of NR2B-deficient neurons and obviating any biological effects associated with the loss of NR2B. Future iterations of this experiment may more stringently optimize viral delivery in order to achieve maximal Cre recombinase activity within V1 neurons, including those in layers 4 and 6, which were not appreciably infected in our experiment. For instance, the promoter for the murine *Six3* gene has been shown to drive the expression of Cre recombinase in

layer 4 of cortical tissues (Liao and Xu, 2008). Furthermore, the high variances accompanying our small samples sizes (control: n = 2; NR2B KO: n = 3) may similarly obscure any true biological effects of NR2B in potentiating SRP and OSH. Future iterations of this experiment may seek to use larger samples within both the NR2B KO and control groups in order to enhance the power of the experiment, and also assess other titrations of the viruses to ensure that neither causes non-specific pathology. Finally, given the age of the mice used in our experiment (p56-66), selective deletion of NR2B may not have significant physiological consequences if there are relatively few NR2B subunits compared to NR2A subunits; work by Quinlan et al. (1999) suggest that the maximal NR2A/NR2B ratio is achieved at or before postnatal 4 weeks. Indeed, experiments using genetic ablation of NR2A have reported significant changes in ocular dominance plasticity in mice aged p21-34 (Cho et al., 2009; Philpot et al., 2007), which have an average NR2A/NR2B ratio of approximately 1 (Quinlan et al., 1999). Future iterations of our experiment here my opt to include younger *Grin2b*$^{fl/fl}$ mice (p21-34 or younger) in order to capture a larger biological effect associated with NR2B ablation.

5.3 High concentration DMSO occludes the acquisition, but not the consolidation, of visual memory

In order to further characterize the function of NR2B in SRP and OSH, we also inhibited NR2B using CP-101,606, a selective NR2B antagonist whose precise binding profile has not been fully elucidated. Preliminary work indicates that CP-101,606 binds at the interface between NR2B and NR1 and interacts with Tyr-109, Gly-112, Ser-132, and Ile-133 on NR1 and Gln-110 on NR2B (**Fig. 15B**) (Burger et al., 2012). CP-101,606 is a structural analog of ifenprodil, a negative allosteric modulator of NR2B, and differs by the shorter linker region and additional hydroxyl group (**Fig. 15D**). These differences may contribute to the tighter binding at the NR1/NR2B interface and the resulting 2.5-fold higher potency than ifenprodil. IC_{50} and K_D values of CP-

101,606 inhibition of NR2B-containing NMDA receptor have previously been reported to be 0.0039 μM (**Fig. 15D**) and 4.2-12.0 nM *in vivo*, respectively, suggesting that CP-101,606 is a potent inhibitor of NR2B (Burger et al., 2012; Chazot et al., 2002; Mott et al., 1998).

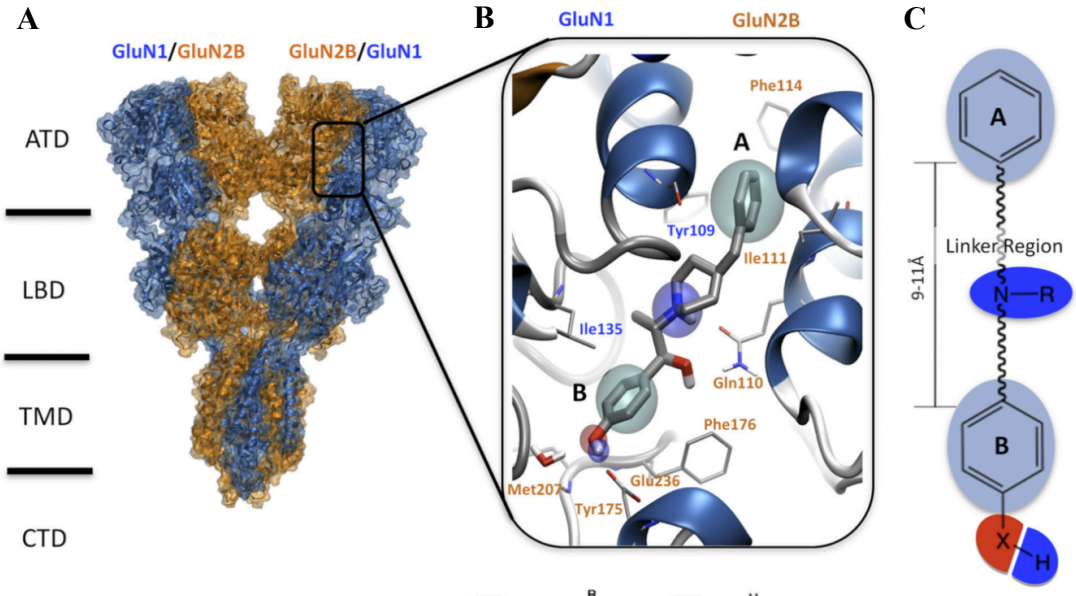

D

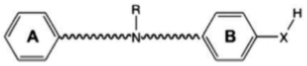

Compound	Structure	IC_{50}
		μM
Ifenprodil	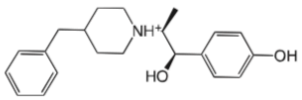	0.040
Ro-25-6981	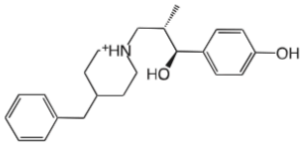	0.009
Traxoprodil	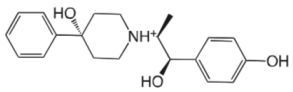	0.0039

Figure 15: Ifenprodil, which is structurally similar to Ro 25-6981 and traxoprodil (i.e., CP-101,606), binds to the GluN1/GluN2B (i.e. NR1/NR2B) interface. (**A**) Structural representation of the NMDA receptor consisting of NR1 and NR2B subunits. ATD, extracellular amino-terminal domain; LTD, extracellular ligand-binding domain; TMD, transmembrane domain; CTD, intracellular carboxyl-terminal domain. (**B**) Close-up of the NR1/NR2B binding interface. CP-101,606 interacts with Tyr-109 (NR1) and Gln-110 (NR2B), as well as Gly-112, Ser-132, and Ile-133 (NR1) (not shown). Ro 25-6981 interacts with Phe-176 (NR2B), as well as Asp-101 and Thr-233 (NR2B) (not shown). Cyan represents the hydrophobic aromatic rings; blue depicts the hydrogen bond donors; red shows the hydrogen bond acceptors. (**C**) Depiction of a general

pharmacophore model for NR2B antagonists, following the same color scheme as (**B**). (**D**) Molecular structures of ifenprodil, Ro 25-6981, and CP-101,606 and corresponding IC_{50} values. Figure adapted from Burger et al. (2012).

During our initial pilot testing, we encountered issues in dissolving CP-101,606 using reported methods including acidified sterile saline (pH 4), serial ethanol dilutions, or low concentration DMSO in sterile water (10% v/v), along with sonication). We obtained a stable drug suspension with a 10% v/v ethanol and 50% v/v glycerol solution but observed no clear effects upon *in vivo* injection prior to SRP training (data not shown). Thus, we subsequently aimed to use a fully solubilized CP-101,606 in a solution of 75% v/v DMSO in sterile water. Interestingly, our observations within the vehicle control group suggest that high DMSO concentration alone may have an effect on potentiation. Indeed, VEP magnitudes measured post-DMSO treatment were higher than those measured prior to DMSO treatment. Moreover, stimuli presented immediately after DMSO treatment failed to potentiate VEPs after the initial training (tested on day 3) while the stimulus presented immediately before DMSO treatment underwent reliable potentiation between days 1 and 3 (**Fig. 13**). Together these data suggest that DMSO blocks the acquisition, but not the consolidation of visual memory. As the same trends were observed in the CP-101,606 treatment group, we were unable to draw any conclusions about the role of NR2B in SRP and OSH (**Fig. 13**).

DMSO is an aprotic solvent that is known to disrupt biological membranes thereby permitting medical applications, including transdermal drug delivery (Notman et al., 2006). To our knowledge, no prior reports have suggested that DMSO has an effect on the potentiation of SRP and OSH. Though prior work on measuring excitatory postsynaptic potentials of NMDA receptors in rat hippocampi demonstrated that low concentration DMSO (0.1% v/v) alone did not produce any biological consequences *in vivo* relative to Propofol dissolved in 0.1% v/v DMSO (Nagashima

et al., 2005), high concentrations DMSO may exhibit neurotoxicity or ocular toxicity, thereby eliminating visual stimulus-specific potentiation.

Interestingly, following the treatment with DMSO, the ability of control mice to undergo SRP was observed again after 3 days (**Fig. 13**), suggesting that the effects of DMSO were transient and cortical activity subsequently recovered. Prior pharmacokinetic characterizations of DMSO in human models suggest that the half-life of DMSO is on the order of magnitude of 11-14 hours (Swanson, 1985). While this reported elimination half-life may not correlate well with mouse physiology, a half-life of 11-14 hours may explain the recovery of VEP potentiation; over 97% of DMSO is eliminated after 5.14 half-lives corresponding to 3 days. While our findings here are fascinating and unexpected, they need to be validated in order to demonstrate that DMSO does have an effect on potentiation. It is worth noting that this potentiation may not be unique to V1 or the acquisition of visual memory; other processes in the brain, beyond the scope of this project, may need to be carefully examined to determine the biological consequences of high concentration DMSO, especially as it concerns medical applications of the drug.

The maximum tolerable dose of DMSO over 24 hours has been reported to be 14 g/kg in mice, while the 24-hour LD_{50} of DMSO has been found to be 20.1 g/kg (Caujolle et al., 1967). Given that even at a dose of 50% v/v, DMSO-induced toxicity, including hemolysis, catatonia, and hypothermia can be observed in mice (Caujolle et al., 1967), we recognize that the absence of SRP and OSH in our mice may be at least partially attributable to physiological consequences of DMSO outside of the brain and eyes. Indeed, new observations from our group have suggested that physical discomfort or malaise resulting from DMSO administration may shift attention and visual processing activities away from visual stimuli, thereby causing larger VEP magnitudes and impairing plasticity (unpublished work).

There may also be alternative explanations independent of DMSO for the control mice exhibiting increased VEP magnitudes post-vehicle-treatment compared to those pre-vehicle-treatment. For instance, the act of intraperitoneal injection may lead to increased sympathetic nervous system activity (e.g., increased heart rate, increased synaptic firing, pupil dilation), thereby affecting visual input processing and potentiating VEP magnitudes. Prior work in the Bear Lab, however, casts doubt on this hypothesis. Frenkel et al. (2006) reported the use of intraperitoneal CPP injections to inhibit NMDA receptors; saline vehicle injections did not potentiate VEPs, suggesting that the act of intraperitoneal injection alone does not affect neurophysiology. A second hypothesis is the fact that showing a mouse two stimuli, one after the other, may potentiate VEPs elicited when viewing the second distinct stimulus. Recent work by other members of our group, however, refute this hypothesis. Cooke et al. (2015) presented mice with two novel stimuli on the same day and did not observe statistically significant differences in VEP magnitudes between the two novel stimuli. In the absence of other plausible explanations, we believe our findings are primarily attributable to the physiological consequences of DMSO.

5.4 Ro 25-6981 inhibition of NR2B shows that NR2B may not necessary for SRP and OSH

Given the numerous methodological issues encountered during our CP-101,606 experiments, we opted to repeat our NR2B inhibition experiment with a second antagonist. Ro 25-6981 is a selective NR2B antagonist that has been used to modulate spatial learning in rats (Clark et al., 2017), and many other forms of learning and plasticity. Biochemically, Ro 25-6981 binds to NR2B and interacts specifically with Asp-101, Phe-176, and Thr-233 residues located within a central cleft of a leucine, isoleucine, valine periplasmic amino acid-binding protein (LIVBP) binding domain found within the amino terminus (**Fig. 15B**) (Burger et al., 2012; Malherbe et al., 2003). Note the structural similarity between Ro 25-6981 and ifenprodil; Ro 25-6981 differs by a chiral

center and an additional carbon atom in the linker region. IC_{50} and K_D values of Ro 25-6981 inhibition of NR2B-containing NMDA receptors have previously been reported to be 0.009 μM (**Fig. 15D**) and 0.003 μM *in vitro*, respectively, suggesting that Ro 25-6981 is potent inhibitor of NR2B (Burger et al., 2012; Fischer et al., 1997; Mutel et al., 1998).

While the effects previously observed using DMSO vehicle were not observed in the saline-treated control group here, we did not observe any statistically significant differences in VEP magnitudes between mice treated with Ro 25-6981 and those treated with a saline control, suggesting that NR2B likely does not play a role in SRP and supporting conclusions drawn from our NR2B knockout experiments above. Interestingly, though we saw no apparent effects of Ro 25-6981 on SRP, we noted that, on average, VEP magnitudes for vehicle-treated mice were marginally larger than those observed in Ro 25 6981-treated mice (not statistically significant), possibly indicating that NR2B may play a role in response sensitivity to visual stimuli. These findings were also observed in NR2B KO mice.

Though statistically insignificant, we observed a large reduction in potentiation from day 3-7 in Ro 25-6981-treated mice relative to control mice in response to the post-drug familiar 75˚ stimulus (**Fig. 14**), potentially suggesting an impairment of visual memory acquisition related to the administration of Ro 25-6981 48 hours prior. Interestingly, the half-life of dissociation of Ro 25-6981 *in vitro* has been reported to be on the order of magnitude of five hours (Mutel et al., 1998), that direct pharmacological inhibition of NR2B likely does not contribute to our observations here. Instead, we hypothesize that the inhibition of NR2B by Ro 25-6981 causes other longer-lasting physiologic changes, such as the compensatory expression of NR2B-containing NMDA receptors to recover normal synaptic signaling, which may contribute to alterations in SRP

and visual memory acquisition. Future experiments are necessary to identify these precise physiologic changes and investigate their causal relationship to SRP.

Cooke et al. (2015) described OSH, which co-occurs with SRP in response to familiar visual stimulus. We were unable to conclusively evaluate OSH in any of the experiments described in this work since the vidget response is inherently variable. Therefore, differences in vidget magnitudes between experimental and control conditions were not statistically significant likely due to the small sample sizes. Differences in vidget magnitudes between stimulation conditions within the same experimental/control groups were also not statistically significant. Our findings reflect a known caveat of OSH, which is not a reliable assay for the acquisition of visual memory in small samples. Future iterations of our experimental approach may opt to replicate the OSH acquisition protocol described here to obtain much larger sample sizes (e.g., n = 15, as described in Cooke et al. (2015)) to better characterize OSH.

6 Future directions

In this volume, we attempted to characterize biochemical changes in NMDA receptor subunit composition during the acquisition of visual memory and the role of NR2B in SRP and OSH. We have already discussed several methodological changes and avenues for further scientific exploration. Importantly, increasing sample size will enhance statistical power, thereby elucidating biological phenomenon from variance. Furthermore, including younger cohorts of mice, which have lower NR2A/NR2B ratios, may enhance biological effects seen during the inhibition of NR2B. Further optimization of vidget acquisition protocols may also improve characterization of OSH.

As one of our incidental observations was a decrease in VEP magnitude in response to Ro 25-6981 inhibition of NR2B, this NMDA receptor subunit may play a role in regulating VEP magnitudes by increasing sensitivity to visual stimuli. We also incidentally observed that stimuli presented immediately after DMSO treatment failed to potentiate VEPs, suggesting that DMSO may inhibit the acquisition of memory. The involvement of NR2B in SRP and OSH is more nebulous, but future experiments may be focused on further characterizing the role of NR2B in visual input processing in V1. As one of our alternative explanations for this phenomenon is the compensatory overexpression of NR2A and NR1, future experiments should also examine gene expression changes in V1 neurons following the loss of NR2B function. Similarly, if the loss of NR2B does cause changes in VEP magnitudes by overexpressing NR2A, future experiments can look for similar phenotypes when NR2A is overexpressed.

7 Conclusions

In summary, NMDA receptor subunit composition in V1 does not appear to change during the acquisition of visual memory in wild-type (p27-29) C57BL/6N mice as determined by the measurement of NR2A and NR2B via Western blot. Given that NMDA receptors are necessary for SRP and OSH (Cooke et al., 2015; Frenkel et al., 2006), we chose to investigate the role of NR2B in these processes. SRP measurements obtained following genetic ablation of NR2B using an intersectional transgenic approach could not conclusively determine if NR2B is necessary for SRP and OSH due to unexpected effects of the control treatment. These results were further clarified by the pharmacological inhibition of NR2B via Ro 25-6981 during training. We observed that Ro 25-6981 injected immediately before or after training had no significant impact on SRP or OSH. Ro 25-6981, however, may have long-term consequences on further induction of SRP days later, which warrants additional testing. Although we were unable to confirm these results using selective NR2B antagonist CP-101,606, we determined that the high concentration of DMSO used as a drug vehicle may prevent the acquisition of visual memory, but not its consolidation. In this work, we have explored aspects of the biochemistry and neurophysiology of NMDA receptor subunit NR2B in the context of visual memory, but our findings are by no means a complete characterization of the protein's function in normal biology and the biological processes that underlie visual memory. Indeed, our experiments with selective NR2B antagonist Ro 25-6981 may suggest that only NR2A-containing NMDA receptors are necessary for SRP. A careful examination of the amino acid differences between NR2A and NR2B as well as the biochemical properties of the two subunits may help to further elucidate the biochemical basis for SRP. Yet, it is important to recognize that as Ro 25-6981 binds to NR2B at the interface between NR2B and NR1 (Chazot et al., 2002; Mutel et al., 1998), other areas of NR2B may still be functional and contribute to biological processes, including SRP. Ultimately, understanding the function and role

of these proteins in visual recognition memory will contribute to a broader appreciation of neuroscience and aid in the development of new therapeutics that target these proteins to enhance or inhibit memory acquisition, consolidation, and recall.

8 References

Balu, D.T. (2016). The NMDA receptor and schizophrenia: from pathophysiology to treatment. In Advances in Pharmacology (Elsevier), pp. 351-382.

Bliss, T.V., and Lomo, T. (1973). Long-lasting potentiation of synaptic transmission in the dentate area of the anaesthetized rabbit following stimulation of the perforant path. The Journal of physiology *232*, 331-356.

Burger, P.B., Yuan, H., Karakas, E., Geballe, M., Furukawa, H., Liotta, D.C., Snyder, J.P., and Traynelis, S.F. (2012). Mapping the binding of GluN2B-selective N-methyl-D-aspartate receptor negative allosteric modulators. Molecular pharmacology *82*, 344-359.

Caujolle, F., Caujolle, D., Cros, S., and Calvet, M.M. (1967). Limits of toxic and teratogenic tolerance of dimethyl sulfoxide. Annals of the New York Academy of Sciences *141*, 110-125.

Chazot, P.L., Lawrence, S., and Thompson, C.L. (2002). Studies on the subtype selectivity of CP-101,606: evidence for two classes of NR2B-selective NMDA receptor antagonists. Neuropharmacology *42*, 319-324.

Cho, K.K., Khibnik, L., Philpot, B.D., and Bear, M.F. (2009). The ratio of NR2A/B NMDA receptor subunits determines the qualities of ocular dominance plasticity in visual cortex. Proceedings of the National Academy of Sciences, pnas. 0808104106.

Clark, E., Antoniak, K., Feniquito, A., and Dringenberg, H.C. (2017). Effects of the GluN2B-NMDA receptor antagonist Ro 25-6981 on two types of behavioral flexibility in rats. Behavioural brain research *319*, 225-233.

Cooke, S.F., and Bear, M.F. (2010). Visual experience induces long-term potentiation in the primary visual cortex. Journal of Neuroscience *30*, 16304-16313.

Cooke, S.F., Komorowski, R.W., Kaplan, E.S., Gavornik, J.P., and Bear, M.F. (2015). Visual recognition memory, manifested as long-term habituation, requires synaptic plasticity in V1. Nature neuroscience *18*, 262.

Fahle, M., and Morgan, M. (1996). No transfer of perceptual learning between similar stimuli in the same retinal position. Current Biology *6*, 292-297.

Fischer, G., Mutel, V., Trube, G., Malherbe, P., Kew, J., Mohacsi, E., Heitz, M., and Kemp, J. (1997). Ro 25–6981, a highly potent and selective blocker of N-methyl-D-aspartate receptors containing the NR2B subunit. Characterization in vitro. Journal of Pharmacology and Experimental Therapeutics *283*, 1285-1292.

Frenkel, M.Y., Sawtell, N.B., Diogo, A.C.M., Yoon, B., Neve, R.L., and Bear, M.F. (2006). Instructive effect of visual experience in mouse visual cortex. Neuron *51*, 339-349.

Furmanski, C.S., Schluppeck, D., and Engel, S.A. (2004). Learning strengthens the response of primary visual cortex to simple patterns. Current Biology *14*, 573-578.

Gilbert, C.D., Sigman, M., and Crist, R.E. (2001). The neural basis of perceptual learning. Neuron *31*, 681-697.

Hebb, D.O. (1947). The effects of early experience on problem-solving at maturity. American Psychologist *2*, 306-307.

Karni, A., and Bertini, G. (1997). Learning perceptual skills: behavioral probes into adult cortical plasticity. Current opinion in neurobiology *7*, 530-535.

Klein, R.L., Dayton, R.D., Leidenheimer, N.J., Jansen, K., Golde, T.E., and Zweig, R.M. (2006). Efficient neuronal gene transfer with AAV8 leads to neurotoxic levels of tau or green fluorescent proteins. Molecular Therapy *13*, 517-527.

Liao, G.Y., and Xu, B. (2008). Cre recombinase-mediated gene deletion in layer 4 of murine sensory cortical areas. Genesis *46*, 289-293.

Liu, X.-B., Murray, K.D., and Jones, E.G. (2004). Switching of NMDA receptor 2A and 2B subunits at thalamic and cortical synapses during early postnatal development. Journal of Neuroscience *24*, 8885-8895.

Malherbe, P., Mutel, V., Broger, C., Perin-Dureau, F., Kemp, J.A., Neyton, J., Paoletti, P., and Kew, J.N. (2003). Identification of critical residues in the amino terminal domain of the human NR2B subunit involved in the RO 25-6981 binding pocket. Journal of Pharmacology and Experimental Therapeutics *307*, 897-905.

Massey, P.V., Johnson, B.E., Moult, P.R., Auberson, Y.P., Brown, M.W., Molnar, E., Collingridge, G.L., and Bashir, Z.I. (2004). Differential roles of NR2A and NR2B-containing NMDA receptors in cortical long-term potentiation and long-term depression. Journal of Neuroscience *24*, 7821-7828.

McBain, C., and Mayer, M. (1994). N-methyl-D-aspartic acid receptor structure and function. Physiological reviews *74*, 723-760.

Menniti, F.S., Shah, A.K., Williams, S.A., Wilner, K.D., White, W.F., and Chenard, B.L. (1998). CP-101,606: An NR2B-Selective NMDA Receptor Antagonist. CNS drug reviews *4*, 307-322.

Monyer, H., Burnashev, N., Laurie, D.J., Sakmann, B., and Seeburg, P.H. (1994). Developmental and regional expression in the rat brain and functional properties of four NMDA receptors. Neuron *12*, 529-540.

Mott, D.D., Doherty, J.J., Zhang, S., Washburn, M.S., Fendley, M.J., Lyuboslavsky, P., Traynelis, S.F., and Dingledine, R. (1998). Phenylethanolamines inhibit NMDA receptors by enhancing proton inhibition. Nature neuroscience *1*, 659.

Mutel, V., Buchy, D., Klingelschmidt, A., Messer, J., Bleuel, Z., Kemp, J.A., and Richards, J.G. (1998). In vitro binding properties in rat brain of [3H] Ro 25-6981, a potent and selective antagonist of NMDA receptors containing NR2B subunits. Journal of neurochemistry *70*, 2147-2155.

Nagashima, K., Zorumski, C.F., and Izumi, Y. (2005). Propofol inhibits long-term potentiation but not long-term depression in rat hippocampal slices. Anesthesiology: The Journal of the American Society of Anesthesiologists *103*, 318-326.

Notman, R., Noro, M., O'Malley, B., and Anwar, J. (2006). Molecular basis for dimethylsulfoxide (DMSO) action on lipid membranes. Journal of the American Chemical Society *128*, 13982-13983.

Paxinos, G., and Watson, C. (1998). A stereotaxic atlas of the rat brain. New York: Academic.
Philpot, B.D., Cho, K.K., and Bear, M.F. (2007). Obligatory role of NR2A for metaplasticity in visual cortex. Neuron *53*, 495-502.

Poggio, T., Fahle, M., and Edelman, S. (1992). Fast perceptual learning in visual hyperacuity. Science *256*, 1018-1021.

Quinlan, E.M., Olstein, D.H., and Bear, M.F. (1999). Bidirectional, experience-dependent regulation of N-methyl-D-aspartate receptor subunit composition in the rat visual cortex during postnatal development. Proceedings of the National Academy of Sciences *96*, 12876-12880.

Sanz-Clemente, A., Gray, J.A., Ogilvie, K.A., Nicoll, R.A., and Roche, K.W. (2013). Activated CaMKII couples GluN2B and casein kinase 2 to control synaptic NMDA receptors. Cell reports *3*, 607-614.

Sawtell, N.B., Frenkel, M.Y., Philpot, B.D., Nakazawa, K., Tonegawa, S., and Bear, M.F. (2003). NMDA receptor-dependent ocular dominance plasticity in adult visual cortex. Neuron *38*, 977-985.

Swanson, B. (1985). Medical use of dimethyl sulfoxide (DMSO). Reviews in clinical & basic pharmacology *5*, 1-33.

Wiesel, T.N., and Hubel, D.H. (1963). Single-Cell Responses in Striate Cortex of Kittens Deprived of Vision in One Eye. J Neurophysiol *26*, 1003-1017.

9 Appendices

Appendix A: Abbreviations

AAV8	Adeno-associated virus serotype 8
ACSF	Artificial cerebrospinal fluid
ANOVA	Analysis of variance
CaMKII	alpha-Ca^{2+}/calmodulin-dependent protein kinase II
CPP	3-(2-carboxypiperazin-4-yl)propyl-1-phosphonic acid
dLGN	Dorsal lateral geniculate nucleus
DMSO	Dimethyl sulfoxide
GFP	Green fluorescent protein
IC_{50}	Half maximal inhibitory concentration
K_D	Equilibrium dissociation constant
KO	Knockout
LD_{50}	Lethal dose, 50%
LTD	Long-term depression
LTP	Long-term potentiation
βME	2-Mercaptoethanol
NMDA	N-methyl-D-aspartate
OSH	Orientation-selective habituation
SDS	Sodium dodecyl sulfate
SEM	Standard error of the mean
SRP	Stimulus-specific response potentiation
TBS	Theta burst electrical stimulation
V1	Primary visual cortex
V2	Secondary visual cortex
VEP	Visually evoked potential
ZIP	Zeta-inhibitory peptide

Appendix B: Supplementary Figures

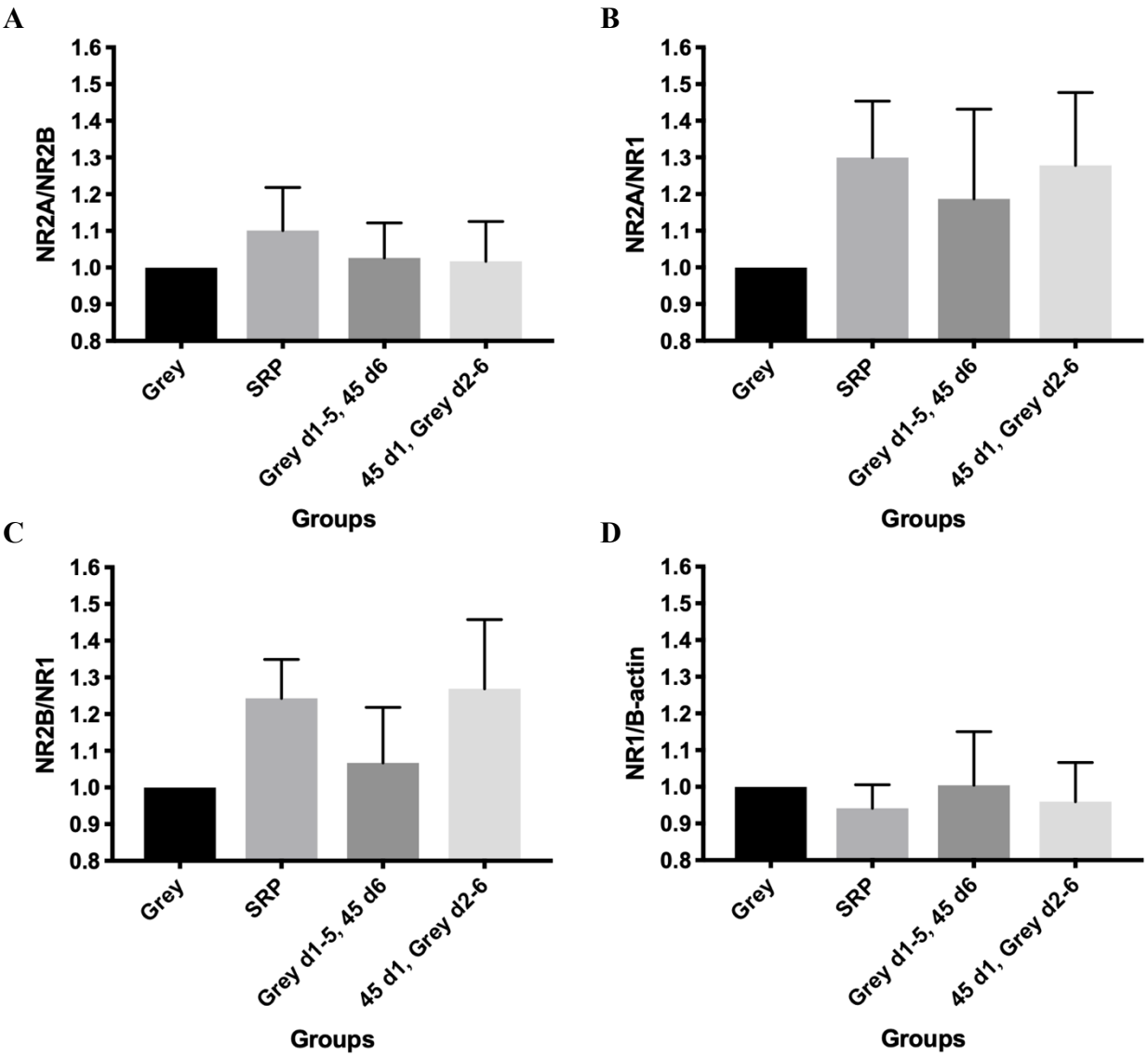

Figure S1: NR2B and NR2A are upregulated in equal proportion in the frontal cortex with increasing visual experience despite no apparent change in total NMDA receptor number. (**A**) The NR2A/NR2B ratio determined via Western Blot of frontal cortical tissue does not differ significantly between control mice shown a grey screen for 6 days, control mice shown a 45˚ grating stimulus on day 1 and grey screen for the subsequent 5 days, control mice shown a grey screen for 5 days and a 45˚ grating stimulus on day 6, and mice shown a 45˚ grating stimulus for 6 days (n = 5). Values reported were calculated as proportion of ratios observed in grey screen control mice. (**B**) The NR2A/NR1 ratio increases in mice shown some visual stimulus relative to mice shown grey screen only. (**C**) The NR2B/NR1 ratio increases in mice shown some visual stimulus relative to mice shown grey screen only. (**D**) The NR1/β-actin ratio remains relatively constant among mice in all groups.

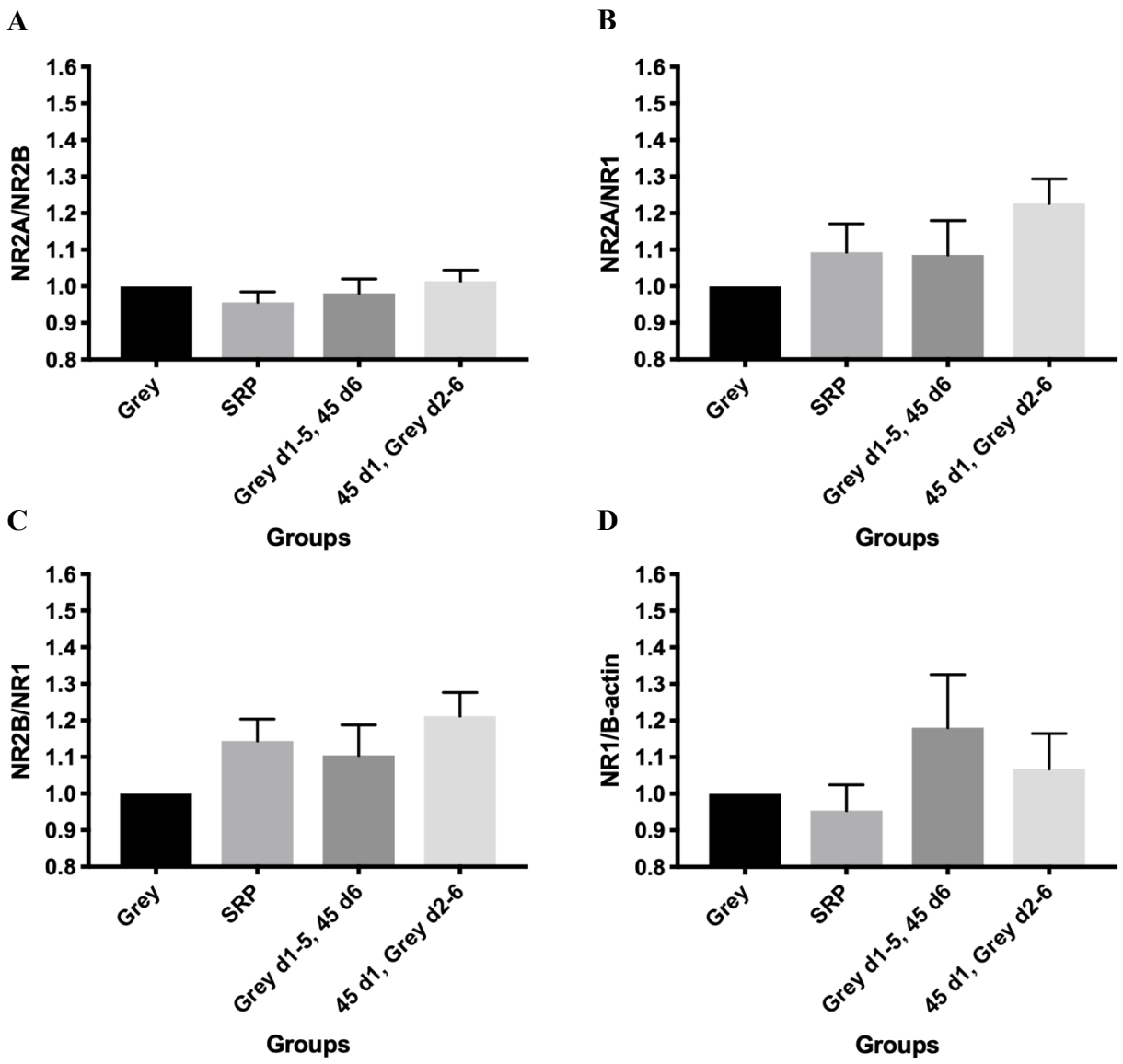

Figure S2: NR2B and NR2A are upregulated in equal proportion in the visual cortex with increasing visual experience despite no apparent change in total NMDA receptor number. (**A**) The NR2A/NR2B ratio determined via Western Blot of visual cortical tissue does not differ significantly between control mice shown a grey screen for 6 days, control mice shown a 45˚ grating stimulus on day 1 and grey screen for the subsequent 5 days, control mice shown a grey screen for 5 days and a 45˚ grating stimulus on day 6, and mice shown a 45˚ grating stimulus for 6 days (n = 5). Values reported were calculated as proportion of ratios observed in grey screen control mice. (**B**) The NR2A/NR1 ratio appears to increase in mice shown some visual stimulus relative to mice shown grey screen only. (**C**) The NR2B/NR1 ratio appears to increase in mice shown some visual stimulus relative to mice shown grey screen only. (**D**) The NR1/β-actin ratio appears to remain relatively constant in mice shown a 45˚ grating stimulus for 6 days (SRP) and control mice shown a 45˚ stimulus on day 1 and grey screen for the subsequent 5 days, while the NR1/β-actin ratio appears to increase in control mice shown a grey screen for 5 days and a 45˚ grating stimulus on day 6.